Fingerprinting the Hydrothermal Fluid Characteristics from LA-ICP-MS Trace Element Geochemistry of Garnet in the Yongping Cu Deposit, SE China

Yu Zhang [1], Qingquan Liu [2,3,*] [ID], Yongjun Shao [3] and Hongbin Li [4]

[1] Key Laboratory of Mineralogy and Metallogeny, Guangzhou Institute of Geochemistry, Chinese Academy of Sciences, Guangzhou 510640, China; zyu2005@csu.edu.cn

[2] School of Resources and Safety Engineering, Central South University, Changsha 410083, China

[3] Key Laboratory of Metallogenic Prediction of Nonferrous Metals and Geological Environment Monitor (Central South University), Ministry of Education, Changsha 410083, China; shaoyongjun@126.com

[4] Graduate School of Engineering and Resource Science, Akita University, Akita 010-0862, Japan; lee_hb@foxmail.com

* Correspondence: liu_qingquan@126.com; Tel.: +86-731-8883-0616; Fax: +86-731-8887-9330

Abstract: The large Yongping Cu deposit is situated in the eastern Qin-Hang Metallogenic Belt, Southeast China and on the southern side of the Yangtze—Cathaysia suture zone, and is characterized by large stratiform orebodies. Garnet represents the main non-metallic mineral at Yongping, and shows variations in color from dark red to green to light brown with distance from the Shizitou porphyritic biotite granite stock. An in situ elemental analysis using EPMA and LA-ICP-MS and fluid inclusions microthermometric measurement on the Yongping garnet were conducted to constrain the hydrothermal and physicochemical mineralization conditions and the ore origin. The Yongping garnet ranges from nearly pure to impure andradite, is characterized by low concentrations of MnO (0.11–0.71 wt %) with a wide range of Y/Ho (2.1–494.9) and does not exhibit any melting inclusions or fluid-melt inclusions, indicating that they are likely to be resulted from hydrothermal replacements. The Yongping garnet is rich in LREEs, Cs, Th, U and Pb; relatively depleted in HREEs, Rb, Sr and Ba; but exhibits distinct Eu anomalies (δEu of the dark red, green and light brown garnet range 2.12–20.54, 0.74–1.70 and 0.52–0.85, respectively) with the homogenization temperatures and salinities of the fluid inclusions principally ranging from 387–477 °C and 7.8–16.0 wt % NaCl equivalent, respectively. The distinct trace elements and microthermometric characteristics reveal that the garnet was formed in a physicochemical conditions of medium-high temperature, 44–64 MPa pressures, mildly acidic pH levels, and unstable oxygen fugacity, and indicate that they were primarily formed by infiltration metasomatism, quite fitting with the scenario that the preferential entrance of magmatic-hydrothermal fluids derived from the Shizitou stock into the relatively low-pressure fracture zones between the limestone and quartz sandstone in the Yejiawan Formation, and further led to the formation of the Yongping stratiform mineralization.

Keywords: trace elements of garnet; fluid inclusion; Yongping Cu deposit; Qin-Hang Metallogenic Belt

1. Introduction

Skarn deposits are a globally important source of Cu, Fe, Pb, Zn, W, Ag, and Au, and the close spatial correlation between the majority of skarn alteration and magmatic intrusions indicates that the skarn minerals can provide a record of ore-forming hydrothermal evolution [1]. Garnet commonly forms during contact metamorphism and hydrothermal alteration of carbonate-bearing rocks and

usually has distinct oscillatory chemical zoning patterns, which can reflect the alteration history during fluid–rock interaction process and provide a continuous record of the physicochemical evolution of the hydrothermal system [2–8]. Based on the rapid development of the electron probe microanalysis (EPMA) and laser ablation inductively coupled plasma mass spectrometry (LA-ICP-MS) in situ testing technologies in recent years, considerable research of garnet has been done on the geochemical ability of garnet to fractionate heavy-group rare earth elements (HREEs) and its high Lu/Hf and Sm/Nd ratios [9–13], and garnet has been widely used to infer the hydrothermal fluid evolution of skarn deposits [3,6,14]. However, such garnet is typically Al-rich garnet (e.g., pyrope, almandine, spessartine and grossular), little attention has been paid to the Fe-rich garnet (e.g., andradite) which is also frequently found in many skarn systems [11,15].

The large Yongping Cu deposit (1.22 Mt Cu with an average grade of 0.77% [16]) is situated in the eastern Qin-Hang Metallogenic Belt in southern China (Figure 1a). The deposit features stratiform orebodies hosted between the limestone and quartz sandstone of the Upper Carboniferous Yejiawang Formation. Extensive research has been conducted on the depositional environment of these ore-hosting strata over the past three decades [17,18], structures [19], metal sources [20–22] and metallogeny of the ore district [23–27]. However, the metallogeny of the Yongping stratiform orebodies has long been controversial over the two major hypotheses are as follows: (1) metallogeny was genetically linked to the Yanshanian magmatic-hydrothermal event(s) related to the Shizitou porphyritic biotite granite stock in the Yongping area [27–32]; or (2) metallogeny was genetically linked to the Hercynian submarine exhalation system and then overprinted by the Yanshanian magmatic-hydrothermal event(s) associated with the Shizitou porphyritic biotite granite stock [16,21,22,33–37]. Both the hypotheses have shed light upon the Yanshanian magmatic-hydrothermal event(s) as which could be acted as an important metallogenic components of the Yongping Cu mineralization, as supported by the ore-forming fluids derived from magmatic waters (H-O isotope data) [22,27], magmatic origin of primary ore-forming material (S-Pb isotope data) [21,22], ore-forming age of Jurassic (Pb-Pb dating of pyrite) [27], together with the extensive skarn alterations (especially garnet) in the Yongping mining area [27,38,39].

Previous studies have paid less attention to the Yongping skarn minerals except for two studies on the major element characteristics [38] and microthermometry [39] of the garnet. Skarn minerals can form via hydrothermal replacement, magmatism, submarine sedimentary exhalation and/or regional metamorphism [1,40,41]. So it still remains unclear whether skarn minerals related to submarine sedimentary exhalation occur at Yongping. Therefore, the origin of the Yongping skarn minerals requires further investigation to constrain the mineralization process. Moreover, although the extensive research on the pressure-temperature (PT) conditions and source of the Yongping ore-forming fluids have been conducted mainly by the fluid inclusions trapped in quartz and calcite [27,37,42,43], little attention had been paid to the hydrothermal fluid evolution of pH and oxygen fugacity, especially during the formation of these skarn minerals.

Detailed field investigations and mineralogical studies of the garnet from the Yongping Cu deposit were performed, and this study presents an in situ analysis of the major and trace elements on garnet using EPMA and LA-ICP-MS, respectively, and microthermometric measurements of the garnet bearing fluid inclusions. The main purpose of this work is to investigate the geochemical characteristics and the genesis of Yongping garnet, constrain the physicochemical conditions of hydrothermal fluids and the ore origin of this large Cu deposit.

2. Geological Setting

2.1. Regional Geology

During the Neoproterozoic Jinning Orogeny at ca. 970 Ma, the Yangtze Block and Cathaysia Block amalgamated along the Jiang-Shao Fault, which promoted the formation of the the South China Block (Figure 1b) [18,27,44–47]. The suture zone between two blocks is relatively active and localizes magmatic-tectonic events. Especially, the northwestward subduction of the Paleo-Pacific plate beneath

the South China Block, since the Early Jurassic, caused widespread Yanshanian volcanic and intrusive magmatism [46,48,49]. The widespread magmatism promoted the extensive mineralization along the suture zone between two blocks, generating the important Qin-Hang Metallogenic Belt in South China (Figure 1a; [46]). The northeastern Jiangxi district, as the important part of eastern Qin-Hang Metallogenic Belt, is characterized by the occurrence of a series of large sized Yanshanian deposits, including the Dexing porphyry Cu deposit which is the largest Cu deposit in eastern China [50], the Yongping Cu deposit, the Tieshajie Cu deposit and the Yinshan Cu polymetallic deposit. The peak ages of the Yanshanian metallogeny in the eastern Qin-Hang Metallogenic Belt range from 170 to 150 Ma which is accordance with the Yanshanian magma emplacement ages [46].
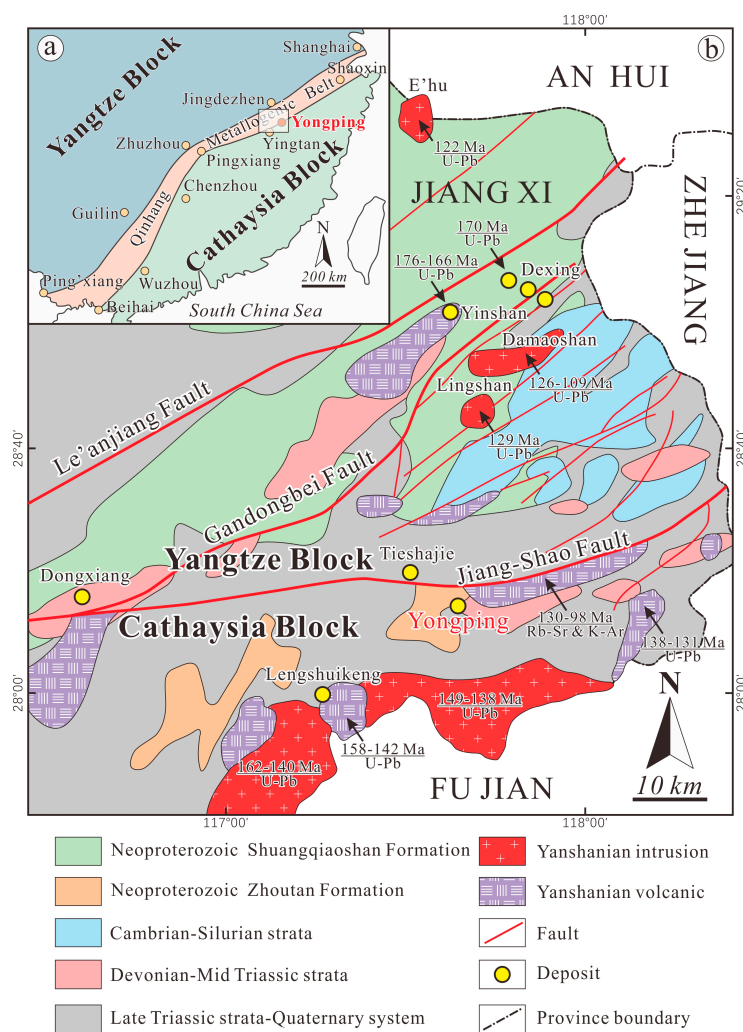
Figure 1. Regional geology of the northeastern Jiangxi district and the location of the Yongping Cu deposit (modified after [27]).

The Jiang-Shao Fault is acted as both the first-order regional deep fault in the district and the suture zone between the Yangtze Block and Cathaysia Block in South China [44], and it is approximately 10 km wide, over 400 km long, dipping to SE and extends to a depth of 90 km. The Gandongbei and Le'anjiang Fault extend over 100 km in length as the regional second-order deep faults (Figure 1b) [27].

The basement strata in the northeastern Jiangxi district include the Neoproterozoic Shuangqiaoshan Formation and Zhoutan Formation. The Neoproterozoic Shuangqiaoshan Formation distribute in the north of the Jiang-Shao Fault and to the southeastern margin of the Yangtze Block (Figure 1b), and it is dominated by shallow sea sedimentary argillo-arenaceous clastic rocks and volcanic clastic rocks [27]

with a depositional age of ca. 860 Ma [51]. Whereas the Neoproterozoic Zhoutan Formation outcrops in the south of the Jiang-Shao Fault and to the northwestern margin of the Cathaysia Block (Figure 2), and it is characterized by a variety of meta-sedimentary and mafic volcanic rocks [52]. The U–Pb data of detrital zircon in the garnet-mica schists reveal that the maximum depositional age of the Zhoutan Formation is ca. 826 ± 5 Ma [52]. Most of rocks in the Zhoutan Formation were migmatized in the Early Paleozoic (446 Ma to 423 Ma) and are unconformably overlain by post-Devonian sediments and intruded by Yanshanian granites [53]. The regional cover strata have ages spanning from Cambrian to Quaternary system, among which Cambrian to Silurian strata is primarily distributed between the Gandongbei Fault and the Jiang-Shao Fault and are mainly composed of terrigenous clastic rocks (Figure 1b) [27]. Devonian to Middle Triassic strata is dominated by sandstone and limestone, and outcrops in the neighborhood area of Gandongbei Fault and Jiang-Shao Fault (Figure 1b) [27].

Yanshanian intermediate to acidic volcanic rocks and granitoids are widely distributed in the northeastern Jiangxi district (Figure 1b). The volcanic rocks outcropping in the south of Jiang-Shao Fault have zircon U-Pb ages of 158–131 Ma and whole-rock Rb-Sr/K-Ar ages of 130–98 Ma [54,55], whereas those in the north of Jiang-Shao Fault exhibit zircon U-Pb ages of 176–166 Ma [56,57]. The large-scale intrusions (e.g., Damaoshan, Lingshan, E'hu) in the northeastern Jiangxi district have younger age (129–106 Ma) and little association with regional mineralization, whereas the small-size intrusions (e.g., Dexing, Yinshan, Dongxiang) have an age of 170–161 Ma and have close relationship with large-scale Yanshanian copper polymetallic mineralization [27,58].

2.2. Ore Deposit Geology

(Meta)-sedimentary rocks at Yongping include those from the Upper Carboniferous Yejiawang Formation to the Lower Permian Chetou Formation, together with minor Neoproterozoic Zhoutan Formation migmatite (Figure 2). The Upper Carboniferous Yejiawang Formation is the main ore-hosting strata, and the stratiform orebodies are confined along the interface between the limestone and the quartz sandstone. The major structures at Yongping include the NNE-trending F1 fault and the Daziping overturned syncline. The Yongping mineralization occurs on the footwall of the F1 fault and in the west limb of the Daziping overturned syncline (Figure 2). The widespread Jurassic granitoids at Yongping primarily include the Shizitou porphyritic biotite granite stock (162 ± 2 Ma) in the southeastern part of the mining area and quartz porphyry dykes (160 ± 2 Ma) and granite porphyry dykes (154 ± 10 Ma) in the western part of the mining area (Figure 2). The granite porphyry dykes locally crosscut the quartz porphyry dykes (Figure 2) [59].

The Yongping Cu orebodies, containing 1.6 Mt of proven copper reserves [27], are mainly stratiform (2500 m long, 2000 m wide and 18 m thick on average), parallel with the Yejiawan Formation and hosted in the facture zones between limestone and quartz sandstone in the Upper Carboniferous Yejiawang Formation (Figure 3) [16]. The limestone in the Upper Carboniferous Yejiawang Formation undergoing alteration to marble and skarn alteration occurs within the hanging walls of the stratiform orebodies, whereas the quartz sandstone acts as the footwall of the stratiform orebodies, in which there are pyrite-bearing quartz stockwork mineralization [26,39]. The orebodies occur in seven NS-trending (east-dipping) mineralization zones (Figure 3). Orebody II-4 is the largest and accounts for 60% of the Cu reserve at Yongping [39].

Field geologic and petrographic observations indicate that metallic minerals are dominated by chalcopyrite and pyrite, with minor scheelite, magnetite, hematite, molybdenite, galena, sphalerite and pyrrhotite. Non-metallic minerals primarily include garnet, diopside, epidote, chlorite, quartz and calcite. Wall-rock alteration styles primarily include the following minerals: garnet, diopside, epidote, sericite, quartz, chlorite and kaolinite [38,39]. Based on the mineral assemblages and textural relationships, mineralization at Yongping occurred in four stages: the prograde skarn (Stage I, garnet + diopside + scapolite), the quartz-pyrite (Stage II, tremolite + quartz + pyrite + magnetite), the quartz-sulfide (Stage III, quartz + sericite + pyrite + chalcopyrite) and the later quartz-calcite-sulfide (Stage IV, quartz + fluorite + chlorite + calcite + pyrite + molybdenite + galena + sphalerite) [27,38,39].
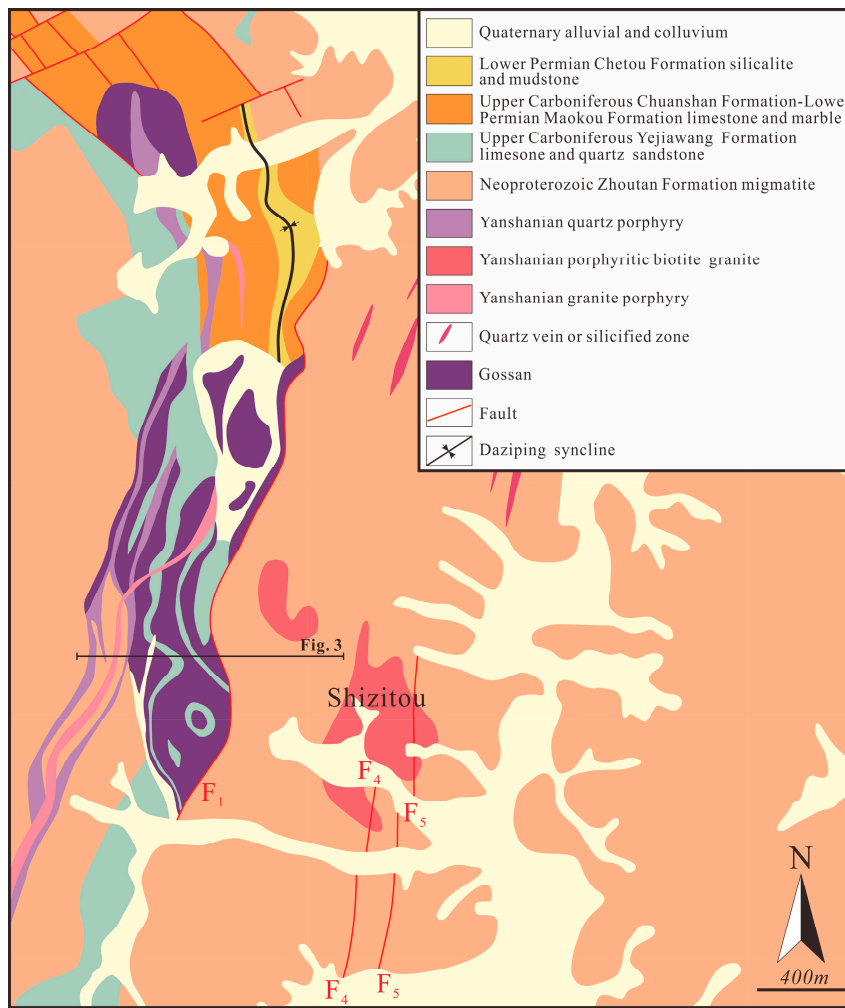
**Figure 2.** Geological map of the Yongping Cu deposit (modified after [60]).
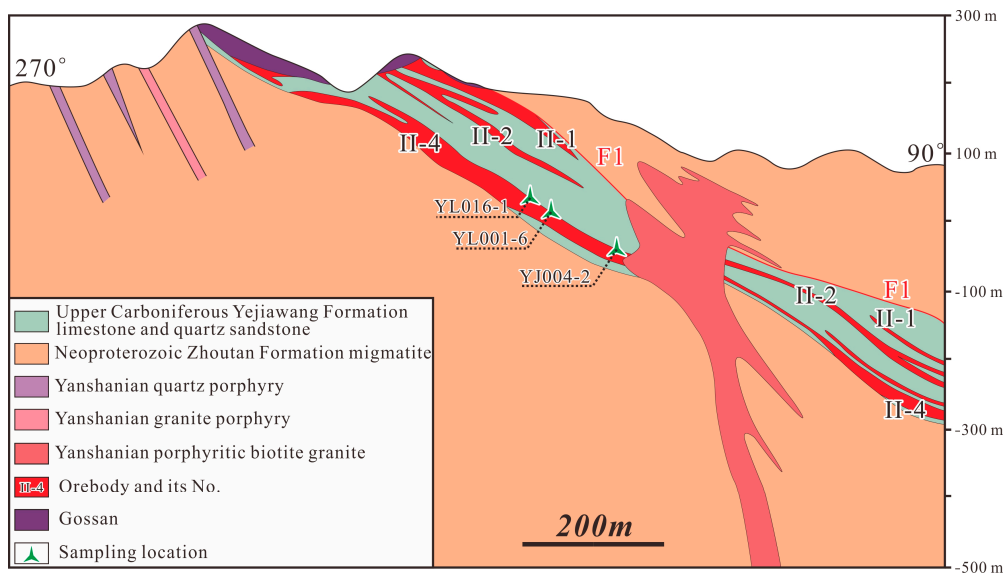
Figure 3. Representative cross-section of the Yongping Cu deposit (modified after [27]).

3. Geology of the Yongping Garnet

Garnet is widely distributed in the hanging walls of stratiform orebodies. Detailed field investigation of garnet revealed that they change in color, from dark red (Figure 4a–c) to green (Figure 4d–f) to light brown (Figure 4g–i), with their distance from the Shizitou porphyritic biotite granite stock. There is no obvious contact interface between the different colors of garnet. The dark red garnet occurs in the hanging walls of the stratiform orebodies proximal to the Shizitou stock (e.g., in the S6-3 (Figure 4a), S5 (Figure 4b) and S6-5 mining tunnels at underground depths of −87 m, −70 m and −50 m, respectively). The dark red garnet co-occurs with trace diopside, chlorite (Figure 4a,b) and epidote (Figure 4a,c) and is locally cut through by calcite veins and pyrite–chalcopyrite–(quartz) veins (Figure 4a,b). The green garnet occurs in the hanging walls of stratiform orebodies near the middle part of the Shizitou stock (e.g., in the east part of the −2 m and 10 m platforms at the Yongping north open pit), has an obvious coarse-grained texture (Figure 4d) and co-occurs with relatively more diopside (Figure 4e). In addition, several pyrite–(chalcopyrite)–quartz veins with chlorites embedded in the sides (Figure 4d,f) crosscut the green garnet (Figure 4d–f). The light brown garnet occurs in the hanging walls of the stratiform orebodies distal from the Shizitou stock (e.g., in the east part of the 22 m and 46 m platforms at the Yongping north open pit), where the light brown garnet locally co-occurs with quartz and calcite in a banded structure (Figure 4g). Further, this banded quartz–calcite–garnet skarn is locally cut through by a quartz vein (Figure 4i) and a pyrite–quartz vein (Figure 4j).
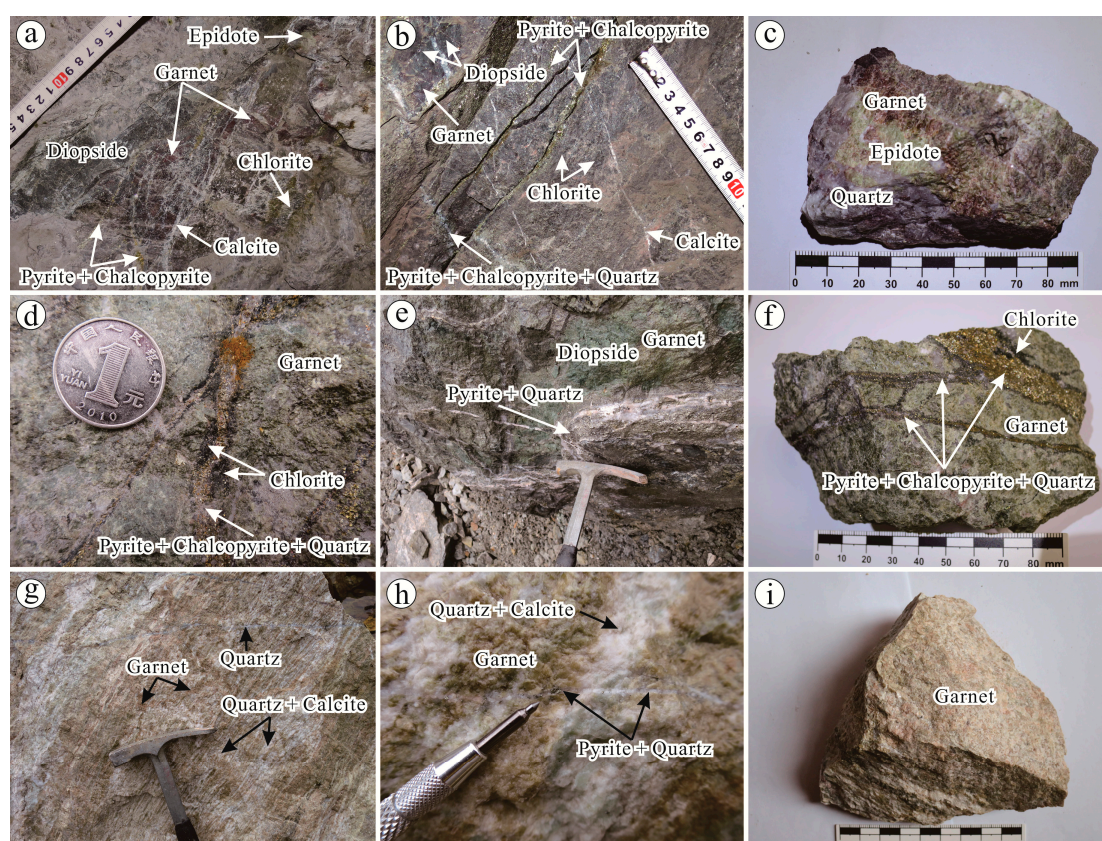
Figure 4. Photographs of Yongping garnet varieties. See text for additional explanation.

4. Sampling and Analytical Methods

The dark red, green and light brown garnet skarn samples were collected in the hanging wall of the No. II-4 stratiform orebody in areas proximal, middle and distal to the Shizitou stock, respectively, specifically in the S5 mining tunnel at an underground depth of −70 m (YJ004-2; Figures 3 and 4c) and at the eastern parts of the 10 m (YL001-6, Figures 3 and 4f) and 22 m (YL016-1, Figures 3 and 4i)

platforms at the Yongping north open pit, respectively. The garnet skarn for sample YJ004-2 contains dark red garnet, epidote and quartz (Figure 4c). Sample YL001-6 contains abundant green garnet and is cut through by pyrite–(chalcopyrite)–quartz veins with chlorite at the sides (Figure 4f). Sample YL016-1 is mainly composed of light brown garnet (Figure 4i).

Sample preparation primarily included laser mount preparation and petrographic microscopy (Leica, Wetzlar, Germany) at the Key Laboratory of Metallogenic Prediction of Nonferrous Metals and Geological Environment Monitor (Central South University), Changsha, China.

The EPMA analysis of the samples, including an in situ major element analysis, EPMA mapping and back-scattered electron (BSE) observations, was performed in the School of Geosciences and Info-Physics of the Central South University using a EPMA-1720 electron probe microanalyzer (Shimadzu Corporation, Kyoto, Japan). The analytical parameters were as follows: 15-kV accelerating voltage, 2.0×10^{-8}-A probe current, 1-μm spot size, and 0.01% detection limit. Every garnet particle was analyzed on multiple spots in an approximate line from core to rim.

Subsequently, a garnet trace element analysis was conducted at the appropriate points analyzed by EPMA using a LA–ICP–MS at the Testing Center of the China Metallurgical Geology Bureau (Shandong office), Jinan, China. Ablation was achieved using a pulsed 193 nm ArF Excimer (COMPexPRO CO2F Geolas; Microlas, Gottingen, Germany), which produced laser power of 8.5 J/cm^2 pulse energy at a repetition rate of 8 Hz, coupled to an Agilent 7500a quadrupole ICP–MS (Aglient, Santa Clara, CA, USA). Helium was used as the carrier gas to provide efficient aerosol transport to the ICP and minimize aerosol deposition. The diameter of the laser ablation craters was 30 μm. The total ablation time was 110 s, which consisted of 30 s for the blank signal, 55 s for ablation, and 25 s for the wash out signal. To correct for laser-induced fractionation, an external standard of NIST 610 glass was analyzed once every 10 analyses to normalize U, Th, Pb, and other trace elements. The resultant data were processed using ICPMSDataCal [61]. The elements analyzed include rare earth elements (REEs) and 13 trace elements (Y, Cs, Rb, Ba, Th, U, Nb, Ta, Pb, Sr, Zr, Hf and Ti).

In addition, the three garnet samples were prepared for fluid inclusion microthermometric measurements. Microthermometric data were obtained using a LINKAM MDSG600 heating–freezing stage (LINKAM, Epsom, UK) coupled to a ZEISS microscope housed in the Key Laboratory of Metallogenic Prediction of Nonferrous Metals and Geological Environment Monitor (Central South University, Changsha, China), Ministry of Education, China. With this instrument, the full range of temperature change was from −196 to +600 °C, and the measurement precision was ±0.1 °C. When measuring the temperature of fluid inclusions, freezing/heating rates were maintained between 0.2 and 5 °C/min, and when nearing a phase transition, the rates were lowered to 0.1–0.5 °C/min. At least 12 fluid inclusions were measured in each sample that presented a sufficient number of inclusions. The microthermometric data were reduced using FLINCOR software by employing the equations of Brown and Lamb [62]. Fluid inclusions trapped in the Yongping garnet were measured to determine their homogenization and final ice melting temperatures. Overall, significant differences were not observed among the fluid inclusions trapped in the garnet from the three samples. The trapped inclusions occur individually or as randomly oriented clusters that are interpreted as primary in origin.

5. Results

5.1. Garnet Petrography

The garnet petrography was investigated using transmitted light microscopy (Leica, Wetzlar, Germany), BSE and EPMA mapping studies.

The dark red garnet is usually euhedral or subhedral and shows distinct oscillatory zoning under the microscope (Figure 5a). The sizes of the grains range mainly from 0.5 mm to 1.5 mm. Locally, dark red garnet grains are cut by calcite veins (Figure 5a) and later fractures (Figure 5b), and they are corroded by anhedral epidote formed at a later stage (Figure 5a,b). In addition, certain garnet

shows a morphological transition from simple dodecahedral {110} growth in the core to composite dodecahedral {110}–trapezohedral {211} growth near the margin in the garnet rims (Figure 5a). The BSE observations reveal that the dark red garnet grains have relatively coarse oscillatory zones that alternate in color intensity from core to rim (Figure 6a,b). The EPMA mapping data indicates that these zones represent the alternating presence of relatively Al-rich and Fe-rich sections (Figure 7). In the BSE images of the garnets, the darker zones are Al-rich and the brighter zones are Fe-rich.
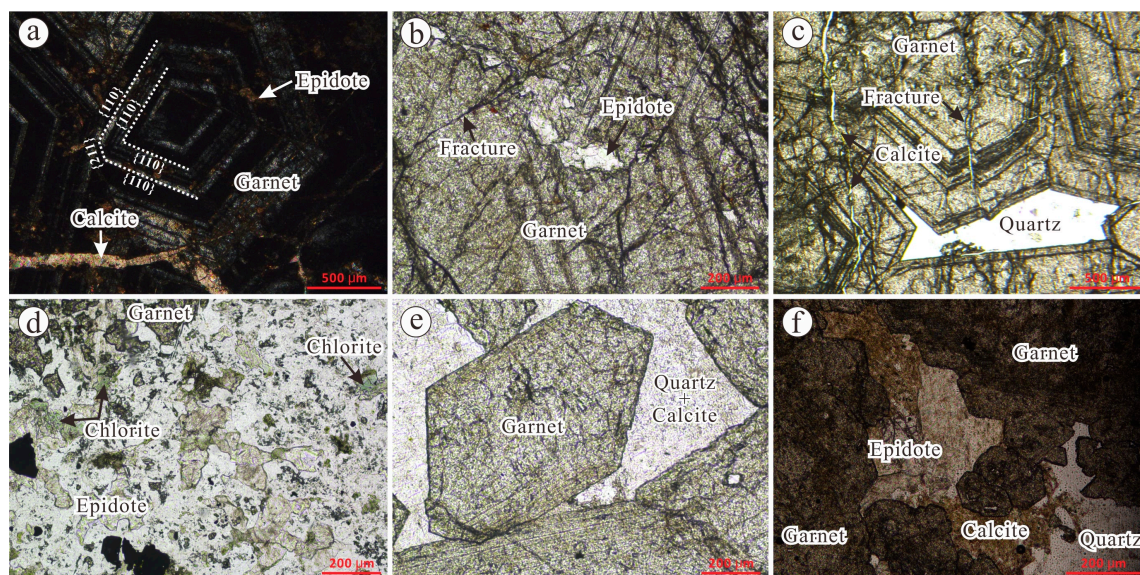

Figure 5. Photomicrographs showing representative textural features of the garnets from the Yongping deposit. (**a**) Dark red garnet particle locally shows a morphological transition from simple dodecahedral {110} growth in the core to composite dodecahedral {110}–trapezohedral {211} growth near its margin in the rim, and it is cut by a calcite vein (CPL); (**b**) dark red garnet particle is locally cut by later fractures and corroded by epidote (PPL); (**c**) green garnet particle has obvious oscillatory zones and is cut by a calcite vein, and the quartz occurring between the garnet particles (PPL) shows an anhedral granular texture; (**d**) green garnet particle with an anhedral granular texture resulted from corrosion by quartz, and the epidote has an anhedral granular texture and is replaced by chlorite (PPL); (**e**) light brown garnet particle with an euhedral granular texture, and calcite and quartz between the garnet particles (PPL); and (**f**) light brown garnet particle with a subhedral granular texture. Epidote, calcite and quartz usually occur between garnet particles, and epidote locally is replaced by calcite (PPL).

The green garnet shows a primarily euhedral granular texture under microscopy (Figure 5c) but with local occurrences of an anhedral granular texture resulting from corrosion by quartz (Figure 5d). The euhedral garnet grains have obvious oscillatory zones (Figure 5c) and various grain sizes ranging from 0.2 mm to 2.0 mm, and they locally occur with a cataclastic texture (Figure 5c). The green garnet co-occurs with epidote, chlorite, quartz and calcite. The epidote usually has an anhedral granular texture and is locally replaced by chlorite (Figure 5d). Calcite often cuts through the garnet grains in the form of veins (Figure 5c). Quartz usually has an anhedral granular texture and locally occurs between the garnet particles (Figure 5c). The BSE images reveal that the green garnet generally is light gray and has extremely fine oscillatory zoning (Figure 6c–e), which is distinct from that of the dark red garnet. In addition, certain green garnet shows a morphological transition from simple dodecahedral {110} growth in the core to composite dodecahedral {110}–trapezohedral {211} growth near the margin in the garnet rims (Figure 6c).
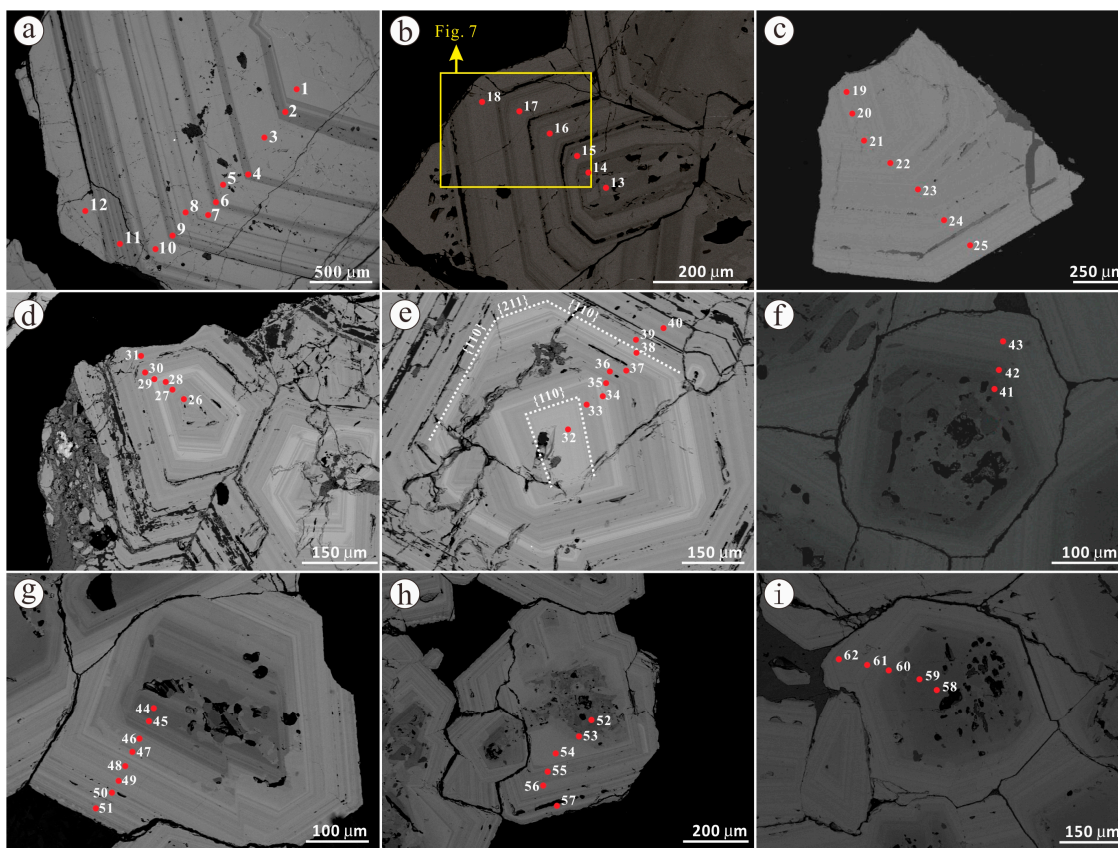
Figure 6. BSE images showing representative textural features of the Yongping garnets. The red spots indicate the spot locations for EPMA and/or LA-ICP-MS analysis and the nearby numbers indicate the spot No. The yellow rectangular frame represents the area for EPMA mapping. (**a**) and (**b**) Dark red garnet with relatively coarse oscillatory zones that present an alternating appearance between the zones, with two different color intensities from core to rim; (**c**,**d**) Green garnet with extremely fine oscillatory garnet zones; (**e**) Green garnet particle with extremely fine oscillatory garnet zones, and a morphological transition from simple dodecahedral {110} growth in the core to composite dodecahedral {110}–trapezohedral {211} growth is observed near its margin in the rim. (**f**–**i**) Light brown garnet cores are dark gray and have no oscillatory zones, whereas the rims are gray and have extremely fine oscillatory zones. The red spots indicate the spot locations for EPMA and/or LA-ICP-MS analysis and the nearby numbers indicate the spot No. The yellow rectangular frame represents the area for EPMA mapping.
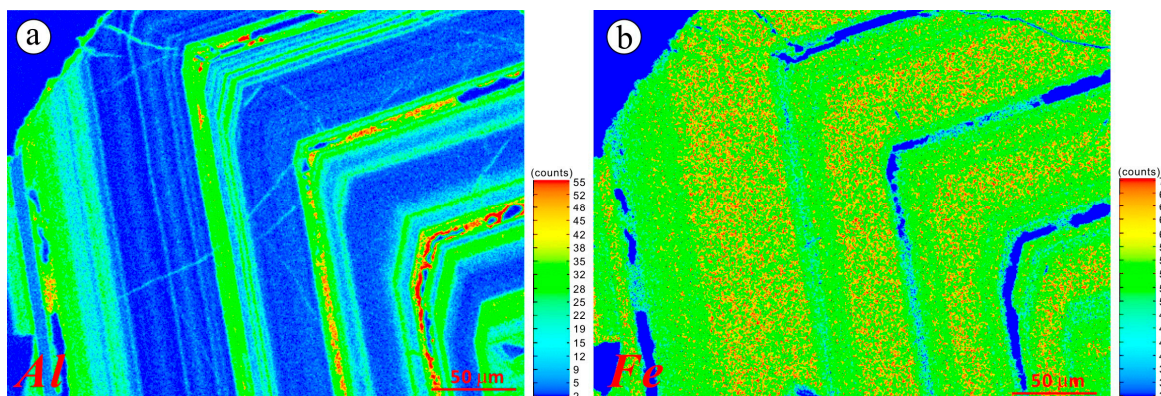

Figure 7. EPMA element mapping of (**a**) Fe and (**b**) Al for a dark red garnet particle.

The light brown garnet is usually euhedral or subhedral and varies in grain size from 0.5 mm to 2.0 mm (Figure 5e,f). Epidote, calcite and quartz usually occur between the garnet particles (Figure 5e,f), and epidote is locally replaced by calcite (Figure 5f). The BSE observations indicated that the cores of the garnet are dark gray and do not have oscillatory zones, whereas the rims are gray and have extremely fine oscillatory zones (Figure 6f–i).

5.2. Major Element Geochemistry

A total of 62 EPMA spot analyses were conducted on representative garnet particles from three samples, including 18 spots on two dark red garnet particles (7 and 11 spots for the relatively Al-rich and Fe-rich zones, respectively), 22 spots on three green garnet particles and 22 spots on four light brown garnet particles. The results (Table 1) indicate that SiO_2, CaO and FeO are the main components of the Yongping garnet, and their concentrations are 32.82–38.15 wt % (average 35.71 wt %), 32.76–36.00 wt % (average 34.16 wt %) and 10.10–28.20 wt % (average 20.01 wt %), respectively.

The EPMA data show that the garnet at Yongping formed from a grossular-andradite solid solution. The garnet is dominated by andradite and grossular with minor amounts of uvarovite, pyrope, spessartine and almandine (Table 1 and Figure 8). In general, the garnet compositions range from nearly pure andradite Ad_{98} to $Ad_{32}Gr_{66}$, with uvarovite, pyrope, spessartine and almandine accounting for less than 2% (Table 1). The zone with a relatively weaker color intensity in the dark red garnet under BSE is nearly pure andradite, whereas the zone with a stronger color intensity is grandite ranging from $Ad_{88}Gr_{11}$ to $Ad_{63}Gr_{36}$ (Table 1 and Figure 8), which is consistent with the EPMA mapping data (Figure 7). The green garnet and the light brown garnet are grandite and exhibit relatively wide content ranges of grossular and andradite, although the green garnet generally presents a greater amount of grossular and less andradite than the light brown garnet (Figure 8).
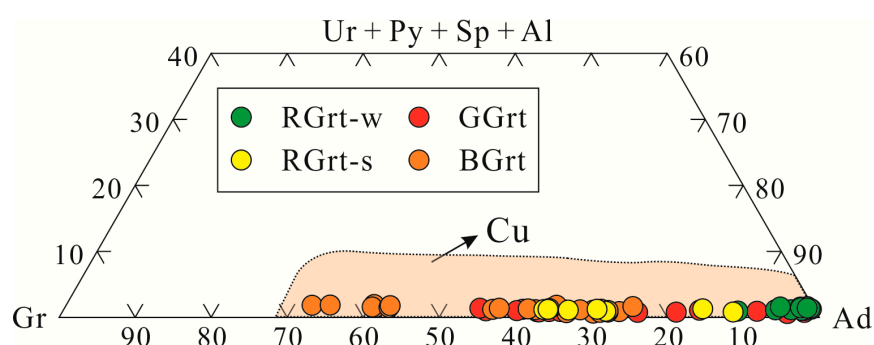
Figure 8. Major element compositions of the garnets showing the dominance of their end members. Colored areas indicate the garnet composition ranges for copper skarn deposits [63]. Abbreviations: Gr = grossular; Ad = andradite; Ur = uvarovite; Py = pyrope; Sp = spessartine; Al = almandine. RGrt-s = zone with stronger color intensity under BSE for dark red garnet; RGrt-w = zone with weaker color intensity under BSE for dark red garnet; GGrt = green garnet; and BGrt = light brown garnet.

Table 1. Representative EMPA geochemical data (wt %) of the Yongping garnet.

Type	Spot No.	SiO$_2$	TiO$_2$	Al$_2$O$_3$	Cr$_2$O$_3$	FeO	MnO	MgO	CaO	Si	Ti	Al	Fe^{3+}	Fe^{2+}	Mn	Mg	Ca	Ur	Ad	Py	Sp	Gr	Al
The dark red garnet sample (YJ004-2)																							
RGrt-w	1	35.18	0.08	0.02	bld	26.99	0.32	0.18	33.09	3.01	0	0	1.93	0	0.02	0.02	3.03	0.01	94.11	0.73	0.74	4.41	0
RGrt-s	2	36.06	0.07	6.80	0.05	19.68	0.29	0.06	34.39	2.96	0	0.66	1.35	0	0.02	0.01	3.03	0.14	66.41	0.22	0.65	32.57	0
RGrt-w	3	35.11	bld	0.19	0.02	27.92	0.25	0.16	33.02	2.98	0	0.02	1.98	0	0.02	0.02	3.00	0.06	97.73	0.68	0.58	0.95	0
RGrt-s	4	35.59	0.07	7.55	bld	18.68	0.37	0.06	33.92	2.95	0	0.74	1.29	0	0.03	0.01	3.01	0	63.69	0.23	0.85	35.19	0.04
RGrt-w	5	34.92	bld	0.09	0.01	27.84	0.21	0.20	33.22	2.97	0	0.01	1.98	0	0.02	0.02	3.03	0.04	96.85	0.81	0.50	1.80	0
RGrt-s	6	35.63	0.01	5.96	0.05	20.55	0.33	0.05	33.96	2.96	0	0.58	1.43	0	0.02	0.01	3.02	0.16	70.14	0.21	0.77	28.72	0
RGrt-w	7	34.36	0.02	0.20	bld	27.80	0.21	0.23	33.14	2.95	0	0.02	1.99	0	0.02	0.03	3.04	0	96.77	0.96	0.50	1.77	0
RGrt-w	8	34.76	0.05	1.44	0.04	25.47	0.14	0.10	33.33	2.98	0	0.15	1.82	0	0.01	0.01	3.06	0.13	88.84	0.40	0.33	10.31	0
RGrt-s	9	36.08	bld	5.47	bld	21.06	0.26	0.06	34.21	2.98	0	0.53	1.46	0	0.02	0.01	3.03	0	71.46	0.24	0.59	27.71	0
RGrt-w	10	34.38	0.05	0.15	bld	27.81	0.19	0.19	32.76	2.96	0	0.02	2.00	0	0.01	0.02	3.02	0	98.16	0.81	0.45	0.59	0
RGrt-s	11	35.31	0.02	7.32	0.02	18.92	0.35	0.06	34.72	2.92	0	0.71	1.31	0	0.02	0.01	3.08	0.05	63.15	0.24	0.80	35.76	0
RGrt-w	12	32.82	bld	0.05	0.05	27.98	0.27	0.18	33.10	2.88	0	0.01	2.05	0	0.02	0.02	3.11	0.17	97.62	0.73	0.64	0.84	0
RGrt-s	13	35.74	0.01	3.28	bld	24.47	0.29	0.07	33.53	2.97	0	0.32	1.70	0.01	0.02	0.01	2.99	0	84.04	0.27	0.67	14.77	0.26
RGrt-s	14	34.14	0.01	2.37	bld	25.22	0.17	0.08	33.21	2.93	0	0.24	1.81	0	0.01	0.01	3.05	0.01	88.27	0.31	0.40	11.00	0
RGrt-w	15	33.87	bld	0.32	0.05	27.09	0.16	0.12	32.83	2.95	0	0.03	1.97	0	0.01	0.02	3.06	0.16	95.74	0.52	0.38	3.20	0
RGrt-w	16	34.64	bld	0.47	0.05	27.04	0.16	0.13	33.49	2.96	0	0.05	1.93	0	0.01	0.02	3.07	0.15	93.69	0.53	0.37	5.26	0
RGrt-w	17	35.24	bld	0.36	bld	27.50	0.21	0.11	32.81	3.00	0	0.04	1.96	0	0.01	0.01	2.99	0	97.19	0.47	0.49	1.85	0
RGrt-w	18	35.44	bld	0.09	0.01	27.87	0.24	0.09	33.11	3.00	0	0.01	1.97	0	0.02	0.01	3.00	0.03	97.63	0.37	0.57	1.40	0
The green garnet sample (YL001-6)																							
GGrt	19	35.47	bld	4.84	bld	22.12	0.23	0.03	33.97	2.96	0	0.48	1.54	0	0.02	0	3.04	0	75.72	0.14	0.53	23.61	0
GGrt	20	33.11	0.01	0.07	bld	27.33	0.11	0.06	33.33	2.91	0	0.01	2.01	0	0.01	0.01	3.14	0	95.54	0.24	0.25	3.98	0
GGrt	21	36.23	0.03	7.01	bld	19.57	0.32	0.02	34.72	2.96	0	0.68	1.34	0	0.02	0	3.04	0	65.45	0.08	0.72	33.75	0
GGrt	22	36.55	0.01	5.99	bld	18.94	0.32	0.02	34.37	3.03	0	0.59	1.31	0	0.02	0	3.06	0	63.99	0.06	0.73	35.22	0
GGrt	23	34.79	0.07	6.78	bld	18.61	0.32	-	34.50	2.93	0	0.67	1.31	0	0.02	0	3.12	0	62.70	0.01	0.72	36.57	0
GGrt	24	37.31	0.06	9.33	bld	16.44	0.54	0.02	34.78	2.99	0	0.88	1.10	0	0.04	0	2.99	0	54.63	0.08	1.21	44.08	0
GGrt	25	35.87	0.02	3.07	bld	23.31	0.30	-	33.54	3.02	0	0.30	1.64	0	0.02	0	3.02	0	80.79	0.01	0.69	18.51	0
GGrt	26	36.16	0.08	8.39	0.01	17.89	0.32	0.05	34.78	2.95	0	0.81	1.22	0	0.02	0.01	3.04	0.03	59.67	0.19	0.71	39.39	0
GGrt	27	35.99	0.13	7.16	0.06	19.16	0.41	0.07	34.57	2.95	0.01	0.69	1.31	0	0.03	0.01	3.04	0.18	64.11	0.26	0.92	34.53	0
GGrt	28	35.36	0.02	3.00	0.05	24.51	0.26	0.06	33.99	2.96	0	0.30	1.71	0	0.02	0.01	3.04	0.16	83.72	0.24	0.59	15.30	0
GGrt	29	34.86	bld	0.20	bld	27.94	0.16	0.07	33.27	2.97	0	0.02	1.99	0	0.01	0.01	3.03	0.01	97.68	0.28	0.37	1.66	0
GGrt	30	36.96	0.01	7.68	bld	18.60	0.31	0.02	34.61	2.99	0	0.73	1.26	0	0.02	0	3.00	0	62.43	0.07	0.70	36.81	0

Table 1. *Cont.*

Type	Spot No.	SiO$_2$	TiO$_2$	Al$_2$O$_3$	Cr$_2$O$_3$	FeO	MnO	MgO	CaO	Si	Ti	Al	Fe^{3+}	Fe^{2+}	Mn	Mg	Ca	Ur	Ad	Py	Sp	Gr	Al
GGrt	31	36.70	0.09	8.94	bld	16.65	0.38	0.01	34.74	2.98	0.01	0.86	1.13	0	0.03	0	3.02	0	55.61	0.05	0.85	43.49	0
GGrt	32	34.53	bld	0.02	bld	27.77	0.16	0.13	33.08	2.97	0	0.00	1.99	0	0.01	0.02	3.04	0	97.38	0.53	0.38	1.70	0
GGrt	33	34.41	0.26	5.65	0.02	20.85	0.39	0.04	34.16	2.90	0.02	0.56	1.47	0	0.03	0.01	3.08	0.07	70.69	0.17	0.90	28.18	0
GGrt	34	35.05	0.03	1.77	0.01	26.54	0.21	0.07	33.71	2.94	0	0.18	1.86	0	0.01	0.01	3.03	0.03	91.37	0.27	0.49	7.80	0.04
GGrt	35	35.81	0.14	5.20	0.00	20.48	0.34	0.04	33.91	3.00	0.01	0.51	1.43	0	0.02	0	3.04	0	70.04	0.15	0.77	29.04	0
GGrt	36	36.51	bld	7.03	0.04	19.61	0.33	0.05	34.57	2.97	0	0.67	1.33	0	0.02	0.01	3.01	0.12	65.78	0.20	0.74	33.16	0
GGrt	37	36.21	0.17	7.18	0.05	18.90	0.29	0.04	34.60	2.97	0.01	0.69	1.29	0	0.02	0.01	3.04	0.15	63.42	0.16	0.65	35.61	0
GGrt	38	33.61	bld	0.31	0.04	28.20	0.20	0.09	33.13	2.90	0	0.03	2.03	0.01	0.01	0.01	3.07	0.12	98.38	0.39	0.47	0.48	0.17
GGrt	39	36.78	0.02	8.42	0.04	18.20	0.35	0.01	34.66	2.97	0	0.80	1.22	0.01	0.02	0	3.00	0	60.35	0.05	0.79	38.51	0.29
GGrt	40	35.80	bld	6.96	0.04	19.50	0.29	0.03	34.62	2.95	0	0.68	1.34	0	0.02	0	3.05	0.12	65.43	0.14	0.65	33.66	0
The light brown garnet sample (YL016-1)																							
BGrt	41	37.59	0.20	13.94	bld	10.74	0.71	0.06	35.64	2.96	0.01	1.29	0.71	0	0.05	0.01	3.01	0	34.67	0.23	1.54	63.56	0
BGrt	42	36.93	0.08	6.63	bld	20.20	0.38	0.05	34.44	2.99	0	0.63	1.37	0	0.03	0.01	2.99	0	67.95	0.19	0.86	30.99	0
BGrt	43	36.57	0.06	5.65	bld	20.70	0.23	0.04	34.01	3.01	0	0.55	1.42	0	0.02	0.00	3.00	0	70.78	0.15	0.52	28.55	0
BGrt	44	37.03	0.08	14.04	0.02	10.10	0.66	0.06	36.00	2.94	0	1.32	0.67	0	0.04	0.01	3.07	0.07	32.30	0.24	1.43	65.96	0
BGrt	45	35.86	0.57	11.76	0.08	13.01	0.51	0.09	35.23	2.91	0.03	1.12	0.88	0	0.03	0.01	3.06	0.23	42.62	0.33	1.12	55.70	0
BGrt	46	37.13	0.25	7.71	0.00	18.40	0.34	0.11	34.88	2.99	0.02	0.73	1.24	0	0.02	0.01	3.01	0	61.03	0.43	0.76	37.78	0
BGrt	47	36.60	0.48	6.62	0.01	19.18	0.36	0.10	34.78	2.98	0.03	0.64	1.31	0	0.02	0.01	3.03	0.04	63.81	0.39	0.81	34.95	0
BGrt	48	36.85	bld	5.87	0.01	21.31	0.29	0.06	34.48	2.99	0	0.56	1.44	0	0.02	0.01	2.99	0.04	71.69	0.26	0.65	27.35	0
BGrt	49	35.34	0.01	5.67	bld	21.26	0.22	0.06	34.42	2.93	0	0.55	1.48	0	0.02	0.01	3.06	0	71.80	0.22	0.49	27.49	0
BGrt	50	36.94	0.01	5.85	bld	20.80	0.20	0.02	34.64	3.00	0	0.56	1.41	0	0.01	0	3.02	0	69.93	0.09	0.46	29.52	0
BGrt	51	36.23	0.06	6.81	0.03	17.00	0.52	0.01	34.39	3.03	0	0.67	1.19	0	0.04	0	3.09	0.09	57.18	0.02	1.18	41.52	0
BGrt	52	35.43	0.30	11.84	0.03	12.85	0.43	0.09	34.87	2.91	0.02	1.14	0.88	0	0.03	0.01	3.07	0.10	42.59	0.36	0.96	55.99	0
BGrt	53	35.66	0.11	7.29	bld	18.87	0.39	0.09	33.31	2.97	0.01	0.72	1.30	0.01	0.03	0.01	2.97	0	64.51	0.37	0.91	33.76	0.46
BGrt	54	35.62	0.00	5.26	bld	22.14	0.29	0.05	33.73	2.96	0	0.51	1.52	0.02	0.02	0.01	3.00	0	74.66	0.19	0.67	23.80	0.68
BGrt	55	34.08	0.00	6.38	bld	20.74	0.31	0.05	34.41	2.87	0	0.63	1.46	0	0.02	0.01	3.10	0	69.70	0.18	0.71	29.31	0.10
BGrt	56	36.37	0.14	6.56	0.03	19.84	0.14	0.05	34.82	2.97	0.01	0.63	1.36	0	0.01	0.01	3.05	0.08	66.37	0.21	0.33	33.01	0
BGrt	57	34.20	0.08	4.74	bld	21.72	0.24	0.05	34.45	2.90	0.01	0.47	1.54	0	0.02	0.01	3.13	0	73.24	0.22	0.56	25.98	0
BGrt	58	38.15	0.34	11.85	0.04	12.47	0.45	0.10	35.70	3.01	0.02	1.10	0.82	0	0.03	0.01	3.02	0.12	40.35	0.37	0.99	58.18	0
BGrt	59	37.51	0.13	11.84	0.07	12.46	0.51	0.13	35.49	2.99	0.01	1.11	0.83	0	0.03	0.02	3.03	0.22	40.43	0.51	1.12	57.73	0
BGrt	60	37.52	0.10	7.99	0.02	16.96	0.34	0.08	34.84	3.04	0.01	0.76	1.15	0	0.02	0.01	3.02	0.06	56.39	0.30	0.76	42.49	0
BGrt	61	36.44	0.48	11.98	bld	12.55	0.50	0.08	35.51	2.93	0.03	1.14	0.84	0	0.03	0.01	3.06	0	40.81	0.31	1.11	57.78	0
BGrt	62	36.59	0.15	7.34	bld	18.54	0.41	0.04	34.62	2.98	0.01	0.71	1.26	0	0.03	0	3.02	0	62.05	0.15	0.92	36.89	0

Note: "bld": Below the detection limit. All the calculations are based on 12 oxygens. Abbreviations: RGrt-s—the zone with stronger colour intensity under BSE of the dark red garnet; RGrt-w—the zone with weaker colour intensity under BSE of the dark red garnet; GGrt—the green garnet; BGrt—the light brown garnet; Ur —uvarovite; Ad—andradite; Py—pyrope; Sp—spessartine; Gr—grossular; Al—almandine.

5.3. Trace Element Geochemistry

The REE data and trace element data for the garnet is shown in Tables 2 and 3, respectively.

The three different colors of garnet from Yongping are characterized by distinct REE patterns (Table 2 and Figure 9). In the dark red garnet, the darker, Al-rich zones under BSE are strongly enriched in light-group REEs (ΣLREEs ranging from 2.24 ppm to 46.76 ppm, average 10.19 ppm), distinctly high ΣLREE/ΣHREE (from 10.30 to 137.08, average 46.09) and La_N/Yb_N ratios (from 6.13 to 304.40, average 69.74), as well as obviously positive Eu anomalies (from 3.00 to 20.54, average 7.83) (Table 2 and Figure 9a). The brighter, Fe-rich zones under BSE have slightly enriched LREEs (ΣLREEs ranging from 1.97 ppm to 5.12 ppm, average 3.44 ppm), relatively low ΣLREE/ΣHREE (from 3.65 to 14.93, average 7.40) and La_N/Yb_N ratios (from 1.31 to 11.91, average 5.14), as well as slightly positive Eu anomalies (2.12 to 9.73, average 3.94) (Table 2 and Figure 9b). Additionally, the REE patterns of Yongping andradite is similar to those in Xinqiao Cu-S-Fe-Au deposit in the Middle-Lower Yangtze River Valley metallogenic belt in eastern China (esp. obvious positive Eu anomaly), which has similar stratiform orebody and ore genesis dispute about skarn-type and SEDEX (Figure 9a) [64]. The green garnet and light brown garnet have the same characteristics with slightly enriched LREEs (ΣLREEs = 13.23–75.85 ppm and 10.56–38.70 ppm, respectively), low ΣLREE/ΣHREE ratios (2.58–54.60 and 1.35–4.84, respectively), and obvious internal fractionation of LREEs (Figure 9c,d). In terms of Eu anomalies, the green garnet shows both negative Eu anomalies (0.74–0.99, average 0.90) and positive Eu anomalies (1.03–1.70, average 1.41), although the light brown garnet has only obvious negative Eu anomalies (0.52–0.85, average 0.68).
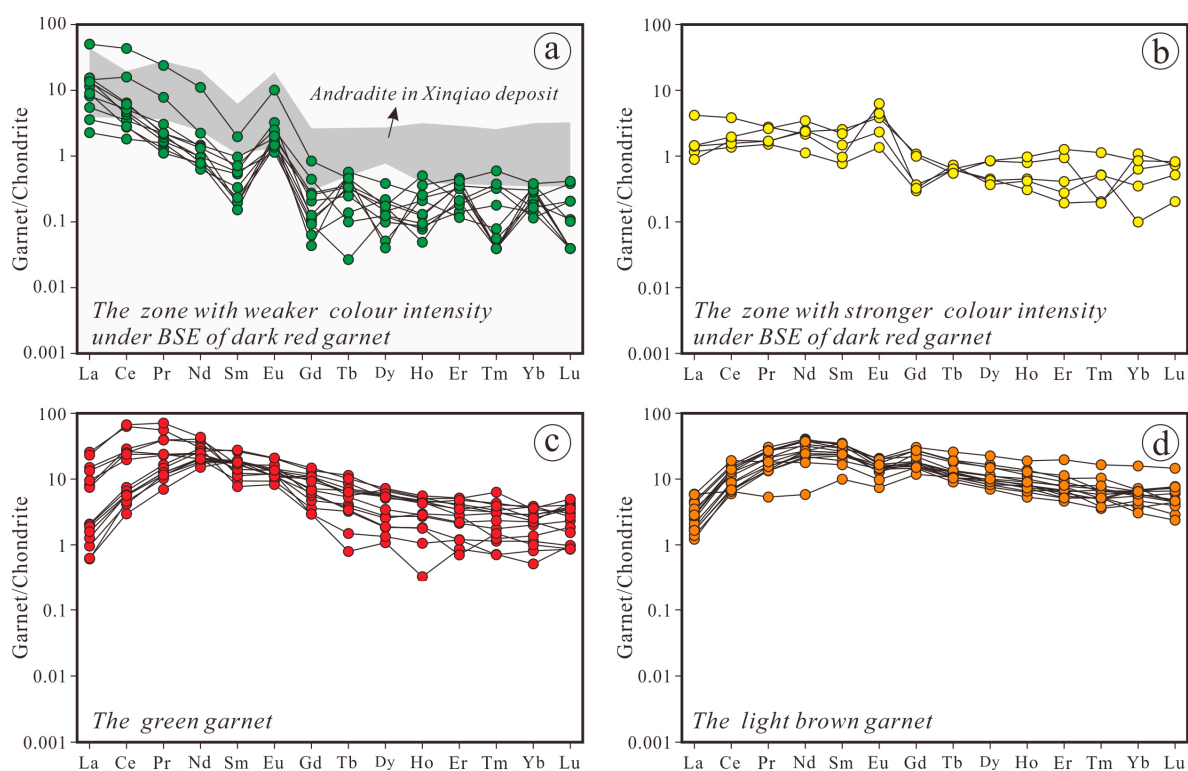

Figure 9. Chondrite-normalized REE patterns of garnets from Yongping. Samples were normalized to the C1 values of Sun and McDonough [65]. The field of Xinqiao andradite is from [64]. (**a**) Zone with stronger color intensity under BSE of dark red garnet; (**b**) zone with weaker color intensity under BSE of dark red garnet; (**c**) green garnet; (**d**) light brown garnet.

Table 2. Representative LA-ICP-MS rare earth elements data (ppm) of the Yongping garnet.

Type	Spot No.	La	Ce	Pr	Nd	Sm	Eu	Gd	Tb	Dy	Ho	Er	Tm	Yb	Lu	ΣREE	ΣLREE	ΣHREE	ΣLREE/ΣHREE	La$_N$/Yb$_N$	δEu	δCe
The dark red garnet sample (YJ004-2)																						
RGrt-w	1	11.930	26.495	2.271	5.173	0.302	0.585	0.173	0.017	0.044	0.029	0.035	0.010	0.028	0.005	47.097	46.756	0.341	137.08	304.40	7.17	1.17
RGrt-s	2	0.343	1.199	0.249	1.612	0.336	0.258	0.204	0.020	0.216	0.055	0.209	0.029	0.144	0.021	4.895	3.996	0.899	4.44	1.70	2.79	0.96
RGrt-w	3	2.122	1.731	0.105	0.364	0.023	0.117	0.009	0.021	0.097	0.014	0.070	0.015	0.065	0.011	4.766	4.463	0.303	14.73	23.47	20.54	0.56
RGrt-s	4	0.336	0.955	0.161	1.103	0.388	0.222	0.221	0.024	0.214	0.045	0.156	0.005	0.184	0.019	4.033	3.165	0.868	3.65	1.31	2.12	1.00
RGrt-w	5	3.196	3.764	0.211	0.618	0.109	0.145	0.092	0.004	0.032	0.005	0.030	0.008	0.052	0.001	8.267	8.043	0.223	36.02	44.36	4.31	0.78
RGrt-s	6	0.990	2.349	0.263	1.005	0.148	0.364	0.067	0.027	0.094	0.024	0.046	0.013	0.060	0.013	5.462	5.119	0.343	14.93	11.91	9.73	1.11
RGrt-w	7	3.670	3.936	0.203	0.373	0.036	0.086	0.053	0.013	0.037	0.012	0.019	0.002	0.057	0.001	8.496	8.303	0.193	42.97	46.33	6.00	0.73
RGrt-w	8	1.937	3.146	0.290	0.643	0.030	0.079	0.013	0.005	0.055	0.007	0.059	0.008	0.019	0.005	6.299	6.126	0.172	35.54	71.47	10.46	0.92
RGrt-s	9	0.211	1.071	0.159	1.149	0.226	0.135	0.075	0.023	0.108	0.025	0.068	0.013	0.017	0.005	3.286	2.950	0.336	8.79	8.94	2.52	1.36
RGrt-w	10	2.717	2.879	0.183	0.451	0.030	0.125	0.043	0.009	0.025	0.005	0.023	0.005	0.024	0.001	6.520	6.385	0.135	47.39	81.99	10.64	0.70
RGrt-s	11	0.277	0.835	0.144	0.523	0.118	0.079	0.061	0.023	0.114	0.017	0.032	0.005	0.108	0.019	2.355	1.974	0.380	5.19	1.85	2.54	1.02
RGrt-w	12	3.389	2.616	0.159	0.457	0.088	0.066	0.019	0.001	0.031	0.004	0.034	0.001	0.031	0.001	6.898	6.776	0.122	55.48	78.42	3.42	0.54
RGrt-w	15	0.539	1.113	0.150	0.294	0.051	0.095	0.026	0.019	0.010	0.020	0.076	0.001	0.063	0.003	2.460	2.242	0.218	10.30	6.13	7.14	0.94
RGrt-w	16	0.849	1.682	0.121	0.344	0.082	0.082	0.021	0.013	0.013	0.013	0.053	0.001	0.048	0.001	3.324	3.160	0.163	19.35	12.60	4.46	1.13
RGrt-w	17	1.301	2.133	0.210	0.686	0.148	0.108	0.056	0.014	0.049	0.007	0.061	0.001	0.039	0.010	4.823	4.587	0.237	19.39	23.92	3.00	0.91
RGrt-w	18	3.417	9.750	0.743	1.042	0.093	0.188	0.023	0.012	0.044	0.003	0.053	0.001	0.033	0.003	15.405	15.234	0.172	88.70	74.05	9.04	1.43
The green garnet sample (YL001-6)																						
GGrt	26	0.376	3.438	1.094	9.455	2.762	0.792	1.900	0.237	1.361	0.243	0.580	0.099	0.430	0.090	22.854	17.916	4.938	3.63	0.63	1.00	0.86
GGrt	27	0.448	3.531	1.200	9.310	2.599	0.640	2.233	0.264	1.522	0.247	0.790	0.110	0.611	0.126	23.631	17.729	5.903	3.00	0.53	0.79	0.79
GGrt	28	3.164	14.569	2.259	11.564	2.146	0.789	1.393	0.199	0.877	0.161	0.365	0.060	0.380	0.039	37.964	34.491	3.473	9.93	5.97	1.31	1.28
GGrt	29	2.258	12.058	2.196	11.114	2.548	0.639	1.269	0.127	0.478	0.101	0.116	0.038	0.170	0.022	33.135	30.813	2.322	13.27	9.53	0.96	1.21
GGrt	30	0.478	4.041	1.395	12.382	4.221	1.212	3.025	0.379	1.831	0.315	0.853	0.103	0.656	0.068	30.960	23.729	7.231	3.28	0.52	0.99	0.79
GGrt	31	0.148	1.811	0.663	7.047	2.926	0.630	2.079	0.234	1.441	0.254	0.463	0.077	0.487	0.091	18.352	13.226	5.126	2.58	0.22	0.74	0.78
GGrt	32	5.478	40.976	6.742	20.236	1.716	0.697	0.603	0.056	0.340	0.060	0.196	0.018	0.138	0.022	77.277	75.845	1.432	52.95	28.47	1.70	1.42
GGrt	33	6.078	38.542	5.285	13.844	1.176	0.479	0.603	0.030	0.274	0.019	0.143	0.018	0.087	0.025	66.602	65.404	1.198	54.60	49.95	1.56	1.55
GGrt	34	1.773	15.345	3.728	18.950	2.522	0.944	1.153	0.137	0.648	0.167	0.463	0.032	0.233	0.047	46.142	43.261	2.881	15.02	5.46	1.47	1.07
GGrt	35	1.930	17.598	3.764	16.851	1.875	0.682	0.970	0.154	0.693	0.153	0.351	0.045	0.341	0.059	45.465	42.700	2.765	15.44	4.06	1.39	1.20
GGrt	36	0.145	2.800	0.969	8.156	2.831	0.777	2.234	0.208	1.755	0.297	0.651	0.078	0.484	0.096	21.482	15.678	5.803	2.70	0.21	0.91	0.85
GGrt	37	0.300	3.526	1.193	9.761	2.897	0.740	1.465	0.251	1.454	0.267	0.690	0.085	0.645	0.102	23.376	18.416	4.960	3.71	0.33	0.98	0.83
GGrt	38	3.555	16.112	2.264	9.435	1.434	0.540	0.739	0.121	0.467	0.103	0.199	0.029	0.193	0.025	35.215	33.339	1.875	17.78	13.24	1.44	1.36
GGrt	39	0.490	4.576	1.569	13.767	4.020	1.193	2.771	0.426	1.664	0.287	0.840	0.161	0.588	0.078	32.431	25.616	6.815	3.76	0.60	1.03	0.80
GGrt	40	0.227	2.542	1.101	8.592	2.899	0.826	2.432	0.323	1.299	0.260	0.566	0.081	0.391	0.111	21.649	16.187	5.462	2.96	0.42	0.93	0.66
The light brown garnet sample (YL016-1)																						
BGrt	41	1.375	11.714	1.733	8.311	2.527	0.567	3.087	0.388	2.546	0.509	1.329	0.202	1.101	0.192	35.582	26.226	9.355	2.80	0.90	0.62	1.59
BGrt	43	0.393	4.213	1.473	11.370	3.639	0.955	3.245	0.396	2.313	0.412	0.855	0.132	0.520	0.060	29.977	22.043	7.934	2.78	0.54	0.83	0.80
BGrt	45	1.401	3.977	0.506	2.720	1.523	0.430	2.424	0.400	2.086	0.370	1.138	0.148	1.101	0.167	18.390	10.556	7.834	1.35	0.91	0.68	1.16
BGrt	47	0.676	8.591	2.544	17.429	5.227	1.144	5.595	0.707	3.775	0.731	1.873	0.170	1.112	0.196	49.769	35.611	14.159	2.52	0.44	0.64	0.95
BGrt	48	0.656	7.863	2.486	17.677	4.527	1.178	4.516	0.506	2.871	0.520	1.291	0.180	1.005	0.118	45.394	34.387	11.006	3.12	0.47	0.79	0.89

Table 2. *Cont.*

Type	Spot No.	La	Ce	Pr	Nd	Sm	Eu	Gd	Tb	Dy	Ho	Er	Tm	Yb	Lu	ΣREE	ΣLREE	ΣHREE	ΣLREE/ΣHREE	La$_N$/Yb$_N$	δEu	δCe
BGrt	49	0.496	5.399	1.682	12.416	3.853	0.845	3.268	0.439	2.479	0.454	1.118	0.097	0.793	0.100	33.437	24.690	8.747	2.82	0.45	0.71	0.89
BGrt	50	0.427	5.240	1.494	10.737	3.613	0.875	3.704	0.488	2.820	0.571	1.268	0.128	1.224	0.109	32.698	22.386	10.312	2.17	0.25	0.72	0.98
BGrt	53	0.833	6.812	1.993	15.766	4.508	1.199	6.244	0.965	5.724	1.071	3.254	0.421	2.688	0.370	51.847	31.111	20.736	1.50	0.22	0.69	0.91
BGrt	55	0.329	3.656	1.276	10.253	2.899	0.824	2.991	0.338	1.781	0.300	0.763	0.091	0.701	0.073	26.276	19.237	7.039	2.73	0.34	0.85	0.81
BGrt	56	0.579	7.747	2.002	12.473	3.846	0.746	5.033	0.673	3.853	0.649	1.509	0.167	1.003	0.123	40.404	27.393	13.011	2.11	0.41	0.52	1.08
BGrt	58	1.014	9.286	2.584	18.298	5.323	0.971	3.802	0.407	2.083	0.451	1.063	0.174	0.940	0.153	46.550	37.476	9.074	4.13	0.77	0.63	0.96
BGrt	59	1.091	9.901	2.902	18.971	4.960	0.878	3.629	0.374	1.915	0.356	0.848	0.134	0.625	0.113	46.698	38.703	7.995	4.84	1.25	0.60	0.92
BGrt	60	0.759	8.559	2.599	14.961	4.031	0.752	3.656	0.467	2.264	0.424	1.024	0.125	1.166	0.194	40.979	31.661	9.319	3.40	0.47	0.59	0.92
BGrt	61	0.288	4.093	1.315	12.493	5.379	1.011	5.649	0.723	4.188	0.776	1.695	0.264	1.155	0.183	39.213	24.579	14.634	1.68	0.18	0.56	0.89
BGrt	62	0.390	4.366	1.268	9.755	3.459	0.877	3.193	0.475	2.409	0.470	0.920	0.128	0.943	0.114	28.767	20.116	8.651	2.33	0.30	0.79	0.95

Note: REE normalized to chondrite [65]. Abbreviations: RGrt-s—the zone with stronger colour intensity under BSE of the dark red garnet; RGrt-w—the zone with weaker colour intensity under BSE of the dark red garnet; GGrt—the green garnet; BGrt—the light brown garnet.

Table 3. Representative LA-ICP-MS trace elements data (ppm) of the Yongping garnet.

Type	Spot No.	Cs	Rb	Ba	Th	U	Nb	Ta	Pb	Sr	Zr	Hf	Y	Ti
The dark red garnet sample (YJ004-2)														
RGrt-w	1	bld	bld	bld	0.157	5.196	0.183	0.006	0.174	0.183	0.407	0.039	0.633	35.355
RGrt-s	2	bld	bld	0.021	0.589	0.305	0.630	0.054	0.033	0.202	24.723	0.655	2.171	159.850
RGrt-w	3	bld	bld	bld	0.193	0.785	0.076	0.003	0.048	0.071	0.800	0.024	0.999	13.264
RGrt-s	4	0.008	0.080	0.881	0.462	0.297	0.495	0.048	0.893	2.902	10.361	0.289	1.811	110.681
RGrt-w	5	bld	0.125	bld	0.089	0.900	0.029	0.003	0.071	0.200	bld	0.031	0.508	6.116
RGrt-s	6	0.054	0.131	bld	0.357	0.620	0.210	0.022	1.436	0.043	2.267	0.118	1.115	34.645
RGrt-w	7	0.187	bld	bld	0.048	1.056	0.013	0.007	0.144	0.069	bld	0.042	0.366	2.430
RGrt-w	8	0.046	bld	0.023	0.106	0.892	0.030	0.002	0.195	0.129	0.828	0.031	0.483	9.802
RGrt-s	9	0.044	bld	0.032	0.366	0.306	0.212	0.021	0.011	0.039	4.867	0.151	1.211	63.277
RGrt-w	10	0.090	bld	0.092	0.048	1.077	0.107	0.003	0.339	0.085	bld	0.027	0.192	3.678
RGrt-s	11	bld	bld	bld	0.278	0.394	0.197	0.012	0.139	0.054	3.122	0.035	0.621	32.078
RGrt-w	12	0.063	bld	0.120	0.046	1.237	bld	0.003	0.099	0.039	bld	bld	0.165	10.279
RGrt-w	15	bld	bld	0.168	0.081	0.392	0.015	0.021	0.289	0.946	0.642	0.036	0.825	14.664
RGrt-w	16	0.010	bld	0.108	0.028	0.620	bld	bld	0.023	0.078	0.633	0.015	0.504	2.504
RGrt-w	17	0.089	bld	bld	0.105	0.952	0.003	bld	0.100	0.221	0.348	bld	0.248	23.262
RGrt-w	18	bld	0.279	0.165	0.105	1.866	0.015	0.008	0.214	0.091	bld	0.025	0.037	21.382

Table 3. *Cont.*

Type	Spot No.	Cs	Rb	Ba	Th	U	Nb	Ta	Pb	Sr	Zr	Hf	Y	Ti
The green garnet sample (YL001-6)														
GGrt	26	0.037	0.570	0.121	1.200	2.144	1.959	0.076	4.222	0.206	16.097	0.305	7.957	406.985
GGrt	27	0.549	0.948	0.385	1.060	2.137	2.112	0.084	2.380	1.177	14.637	0.342	8.936	384.802
GGrt	28	bld	0.227	bld	0.643	7.052	0.846	0.036	0.319	0.065	3.867	0.104	4.853	140.313
GGrt	29	bld	0.075	0.030	0.846	6.083	0.373	0.032	0.232	0.122	1.831	0.032	3.111	71.620
GGrt	30	0.083	0.516	0.121	0.472	1.861	1.826	0.027	0.556	0.098	9.062	0.101	10.001	338.256
GGrt	31	0.040	bld	0.143	0.500	0.885	1.803	0.060	0.422	0.089	2.638	0.025	6.350	295.509
GGrt	32	bld	bld	0.126	1.817	15.746	0.061	bld	0.508	0.157	4.741	0.190	2.342	16.990
GGrt	33	bld	0.325	0.022	0.851	14.951	0.040	0.008	0.537	0.131	5.084	0.115	1.510	8.729
GGrt	34	bld	0.036	bld	2.954	5.571	1.538	0.042	0.392	0.210	11.982	0.206	5.739	342.657
GGrt	35	0.013	bld	0.217	2.472	6.176	0.945	0.046	0.233	0.132	5.624	0.238	5.441	231.789
GGrt	36	bld	0.275	0.353	0.781	1.459	2.172	0.093	0.116	0.201	11.692	0.234	9.020	376.671
GGrt	37	bld	bld	0.085	1.530	2.511	2.128	0.105	0.160	0.023	19.905	0.352	7.886	461.995
GGrt	38	0.216	bld	0.008	0.677	8.117	0.533	0.015	0.339	0.118	4.196	0.032	2.924	77.034
GGrt	39	0.221	0.485	0.139	0.717	2.078	1.537	0.072	0.626	0.005	7.243	0.154	10.403	289.238
GGrt	40	0.035	bld	0.329	0.962	1.208	1.767	0.060	0.332	0.052	6.625	0.087	6.991	290.399
The light brown garnet sample (YL016-1)														
BGrt	41	0.038	0.298	0.096	1.478	1.373	3.335	0.311	0.366	0.646	16.935	0.469	19.202	1166.644
BGrt	43	bld	0.204	bld	2.334	0.444	2.514	0.067	0.045	0.083	6.704	0.147	12.778	566.489
BGrt	45	0.140	0.012	bld	0.247	0.455	2.555	0.375	3.733	0.060	15.098	0.457	16.386	1215.283
BGrt	47	0.041	bld	0.107	5.144	1.519	6.588	0.840	0.128	0.019	30.998	0.929	24.127	2885.790
BGrt	48	bld	bld	bld	5.338	1.252	4.989	0.446	0.051	0.071	21.322	0.410	17.363	1807.104
BGrt	49	0.020	bld	0.134	1.940	0.578	3.503	0.109	0.086	0.049	7.357	0.113	15.256	566.911
BGrt	50	0.606	0.964	0.020	1.360	0.475	3.138	0.175	0.105	0.262	5.599	0.108	18.336	500.789
BGrt	53	0.833	1.078	1.538	13.046	1.697	9.745	0.896	5.299	1.352	44.784	0.924	39.893	3231.003
BGrt	55	0.083	0.038	bld	1.736	0.430	2.495	0.063	0.012	0.100	5.432	0.152	10.972	567.383
BGrt	56	bld	0.554	0.099	2.676	0.649	3.863	0.088	0.129	0.004	5.649	0.096	22.590	434.915
BGrt	58	0.861	1.015	0.407	6.382	1.816	5.691	0.354	4.164	2.279	27.435	1.249	15.929	875.278
BGrt	59	0.401	0.822	0.620	6.625	1.935	2.700	0.056	2.278	3.902	10.371	0.363	12.802	387.922
BGrt	60	1.504	3.004	0.456	2.438	1.200	2.803	0.294	1.837	1.419	12.815	0.301	16.551	939.071
BGrt	61	bld	0.325	bld	1.011	0.637	2.747	0.256	0.253	0.075	18.397	0.561	25.687	1903.033
BGrt	62	0.004	bld	bld	1.044	0.464	3.367	0.181	12.834	1.401	10.837	0.076	15.666	583.014

Abbreviations: RGrt-s—the zone with stronger colour intensity under BSE of the dark red garnet; RGrt-w—the zone with weaker colour intensity under BSE of the dark red garnet; GGrt—the green garnet; BGrt—the light brown garnet.

In general, the three variations of Yongping garnet is depleted in large ion lithophile elements (LILE) and Rb, Sr and Ba relative to primitive mantle [65] (Table 3 and Figure 10). In contrast, the Cs, Th, U and Pb in the Yongping garnet are generally enriched relative to the Cs, Th, U and Pb in the primitive mantle (Table 3 and Figure 10).
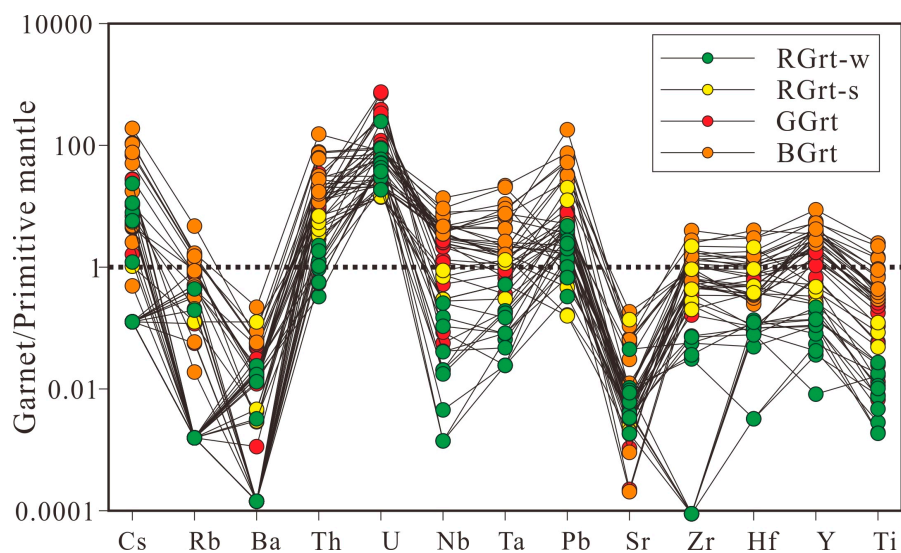

Figure 10. Trace element spider diagram of garnets from Yongping. Samples were normalized to the primitive mantle values [65].

5.4. Microthermometric Results from Fluid Inclusions

The shapes of the fluid inclusions generally include elliptical, negative crystal, elongate, or irregular forms (Figure 11). The majority of the fluid inclusion populations are aqueous Liquid–Vapor (L–V) inclusions (15–55 vol % vapor, 4–22 μm in size, Table 4 and Figure 11), and melt inclusions or fluid-melt inclusions were not found in any of the garnet particles measured. The heating and freezing data show that the homogenization temperatures (Th) principally range 387–477 °C, 415–434 °C and 403–455 °C for the garnet from YJ004-2, YL001-6 and YL016-1, respectively (Table 4 and Figure 12a). Further, the salinities of the fluid inclusions trapped in garnet from YJ004-2, YL001-6 and YL016-1 range from 8.5 to 16.0 wt % NaCl equivalent, from 8.7 to 14.5 wt % NaCl equivalent and from 7.8 to 16.0 wt % NaCl equivalent, respectively (Table 4 and Figure 12b), and their estimated densities range from 0.57 to 0.71 g/cm^3, from 0.57 to 0.67 g/cm3 and from 0.59 to 0.68 g/cm3, respectively (Table 4). In general, the homogenization temperatures and salinities of the primary fluid inclusions hosted in the Yongping garnet mainly range from 410 to 460 °C and from 12.0 to 16.0 wt % NaCl equivalent, respectively (Figure 12).
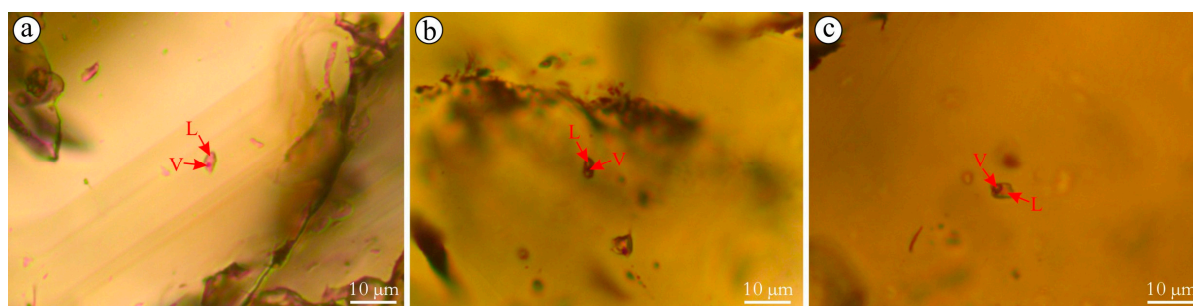
Figure 11. Photomicrographs of the L–V-type fluid inclusions trapped in (**a**) dark red garnet, (**b**) green garnet and (**c**) light brown garnet.

Table 4. Fluid inclusion microthermometric data of the garnet from Yongping Cu deposit.

Sample	Origin	N	Type	Size (µm)	V/(V + L) (%)	Tm-ice (°C)	Th (°C)	Salinity wt % NaCl Equivalent	Density (g/cm³)
YJ004-2	P	11	L–V	4.2 to 22.1	20 to 40	−12.0 to −5.5	387 to 477	8.5 to 16.0	0.57 to 0.71
YL001-6	P	14	L–V	4.4 to 14.7	15 to 55	−10.5 to −5.6	415 to 434	8.7 to 14.5	0.57 to 0.67
YL016-1	P	13	L–V	4.8 to 22.2	18 to 40	−12.0 to −5.0	403 to 455	7.8 to 16.0	0.59 to 0.68

Abbreviations: P is primary, V is vapor, L is liquid, Tm-ice = ice melting temperature, Th = total fluid homogenization temperature, and N is the number of the measured inclusions.
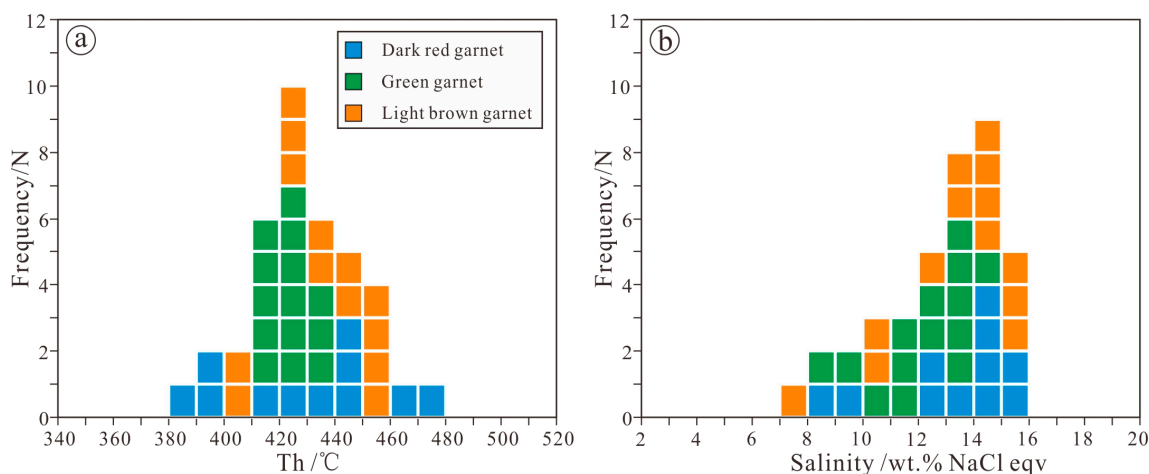
Figure 12. Histograms of the (**a**) homogenization temperatures and (**b**) salinities of the fluid inclusions in the Yongping garnets.

6. Discussion

6.1. Origin of the Yongping Garnet

There is widespread Neoproterozoic Zhoutan Formation migmatite in the Yongping district, and zircon U-Pb dating indicated that the regional metamorphism of the Zhoutan Formation migmatite occurred at 438.2–436.7 Ma [25]. The Yongping garnet generally occurs in the Upper Carboniferous Yejiawang Formation, which indicates that the Yongping garnet formed after the regional metamorphism and is probably not directly linked with the same regional metamorphism that produced the Zhoutan Formation migmatite. Abundant Fe and Mn occur in the seafloor, and garnet from submarine sedimentary exhalation is usually almandine and/or spessartine [66,67]. The Yongping garnet formed from a grossular-andradite solid solution and has low concentrations of MnO (0.11–0.71 wt %, average 0.31 wt %), is inconsistent with garnet from submarine sedimentary exhalation. Melting inclusions and fluid-melt inclusions are considered direct indicators of garnets that originated from magmatism [68–70]; however, these inclusions are not observed in the Yongping garnets. The partial melting or fractional crystallization of magma could not cause Y to fractionate from Ho [71], and the Y/Ho ratio for magmatism is close to the chondrite value (28) [72]. whereas hydrothermal systems can easily fractionate Y from Ho. The dark red garnet, the green garnet and the light brown garnet have Y/Ho ratios ranging from 2.1 to 494.9 (average 90.4), from 25.0 to 81.4 (average 35.2) and from 31.0 to 44.3 (average 35.4), respectively, which suggests that the Yongping garnet likely formed from hydrothermal activity rather than magmatism. Based on that the Yongping garnets are primarily distributed in the hanging walls of the stratiform orebodies that are spatially near the Yejiawan Formation limestone and the Shizitou stock, the garnet should be interpreted as resulting from contact metamorphism during the skarn alteration. This interpretation is consistent with the Yongping garnet that plots in the field defined by garnets from skarn Cu deposits worldwide, as shown in Figure 8. Furthermore, the obvious zonation of the Yongping garnet, which present different colors, from dark

red to green to light brown, with distance from the Shizitou stock, is consistent with the garnet zoning characteristics in worldwide skarn deposits [1]. In accordance with the magmatic-hydrothermal hypothesis for the origin of the Yongping mineralization, the garnet in the hanging walls of the stratiform orebodies should be interpreted as resulting from the interaction between the Yejiawan Formation limestone and magmatic hydrothermal activity that is genetically linked with the Shizitou stock, particularly along the fracture zones between the limestone and quartz sandstone in the Yejiawan Formation [28–32].

6.2. Physicochemical Conditions of Hydrothermal Fluids for Garnet Growth

6.2.1. pH

Bau (1991) [73] demonstrated that pH has a major effect on REE fractionation by hydrothermal fluids. When pH is nearly neutral, the REE pattern of the fluid is relatively HREE enriched and LREE depleted and presents a negative or absent Eu anomaly, whereas in mildly acidic pH, the REE pattern is relatively LREE enriched and HREE depleted and the Eu anomaly is significantly controlled by the presence of complexing agents such as Cl^- [73]. The latter can enhance the stability of soluble Eu^{2+} with respect to REE^{3+} and favor the transportation of Eu^{2+} in hydrothermal fluids and the substitution of Eu^{2+} for Ca^{2+} in garnet crystals, thereby forming distinctly positive Eu anomalies [11,74,75]. The presence of magnetite and hematite, especially magnetite that locally replaces hematite at Yongping [39], indicates a reducing environment with fO_2 below the hematite-magnetite buffer [76]. Under such reduced conditions, Eu should be present as Eu^{2+} [11]. The Eu^{3+}/Eu^{2+} redox potential in hydrothermal fluids is primarily dependent on the temperature and speciation, and at temperatures above 250 °C, Eu^{2+} should predominate in hydrothermal solutions [73,77]. The homogenization temperatures of the fluid inclusions trapped in the Yongping garnet principally range from 387 °C to 477 °C (Table 4). Therefore, Eu mainly occurred as Eu^{2+} in the hydrothermal fluid during the formation of the garnet. Using a gas chromatograph, Cl^- concentrations beyond the detection limit were detected in the fluid inclusion clusters only in the dark red garnet (average 4.137 ppm) and not in the green and light brown garnet [26]. The presence of Eu^{2+} and Cl^- in the hydrothermal fluid for the dark red garnet and the red garnet REE patterns of enriched LREE, depleted HREE and distinctly positive Eu anomalies all imply that the dark red garnet must have crystallized under mildly acidic conditions [11,15]. The slightly LREE-enriched and HREE-depleted green and light brown garnets are inferred to have formed under mildly acidic conditions as well, and their various Eu anomalies may be the result of reduced concentrations of Cl^- in the hydrothermal fluid, consistent with garnet from the Xinqiao Cu–S–Fe–Au deposit [64].

6.2.2. Oxygen Fugacity

The incorporation of U, REE^{3+} and Y into grandite or andradite is possible only by coupled substitution of Ca^{2+} in the dodecahedral position based on the ionic radius [6,11,78,79]. For the element U, U^{4+} is more likely to substitute into garnet than U^{6+} [6]. Thus, the U concentrations in different sections of garnet crystals can indicate the relative oxygen fugacity of hydrothermal fluids during the formation of the crystals. A decreasing fO_2 value in the fluid system could reduce the U solubility and in turn increase the U incorporation into garnet.

In the dark red garnet, the zones with stronger color intensity under BSE have obviously lower U concentrations (0.297–0.394 ppm, average 0.384 ppm) than the zones with weaker color intensity (0.392–5.196 ppm, average 1.361 ppm), which reveals that the dark red garnet must have crystallized during episodic fluctuations between relatively high and low oxygen fugacity in the hydrothermal solutions. Every garnet particle was analyzed by LA-ICP-MS on multiple spots in an approximate line from core to rim (Figure 6 and Table 3), and the results show that the U concentrations from core to rim in every green or light brown garnet are uneven, irregular and variable (Figure 13 and Table 3), thus implying instability of the oxygen fugacity during the crystallization of the green and light

brown garnets. Generally, the U concentrations of the dark red, green and light brown garnets range 0.297–5.196 ppm (average 1.056 ppm), 0.885–15.746 ppm (average 5.199 ppm) and 0.430–1.935 ppm (average 0.995 ppm), respectively, and these data indicate that the oxygen fugacity for the green was likely higher than that for the dark red and light brown garnets.
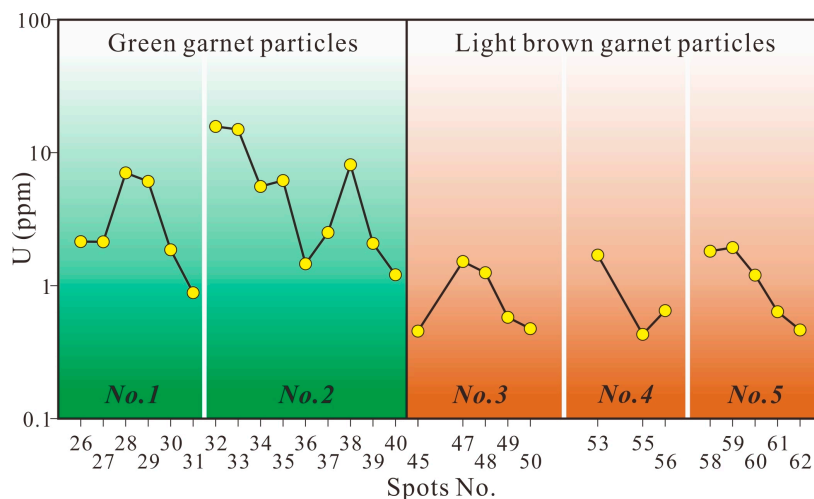

Figure 13. Line chart of the U concentrations from cores to rims in the green and light brown garnet grains; the U concentrations from core to rim in all these grains are irregular.

Garnet is stable only at relatively high temperatures, where it is less likely to leak fluids [80], which favors the preservation of primary inclusions trapped in the garnet crystal. Therefore, the homogenization temperature data of the primary inclusions hosted in garnet are usually applied to calculate the PT conditions of the hydrothermal fluids when the garnet crystallized. All of the calculations were conducted assuming an $H_2O - NaCl \pm CO_2$ fluid system for this study. Fluid boiling was determined according to the criteria outlined by Roedder [81], and it demonstrated that primary fluid inclusions were trapped simultaneously with variable L/V ratios. Accordingly, these fluid inclusions were selected to constrain trapping pressures. We calculated the contours of the fluid trapping pressures as suggested by Driesner and Heinrich [82] plotted them in the constructed homogenization temperature versus salinity diagram (Figure 14). The result shows that the trapping pressures of the primary inclusions in the Yongping garnet ranged between 44 MPa and 64 MPa (Figure 14) corresponding to the homogenization temperatures of 387–477 °C and salinities of 7.8–16.0 wt % NaCl equivalent. Compared with the aqueous L-V fluid inclusion trapped in quartz in Stages II to IV, fluid inclusions trapped in the Yongping garnet has obviously higher fluid trapping pressure, homogenization temperature and salinity (Figure 14). In general, the fluid pressure and temperature exhibit the gradual decrease from Stage I to IV (Figure 14), but the lowest fluid salinity response to the main metallogenic stage (Stage III).
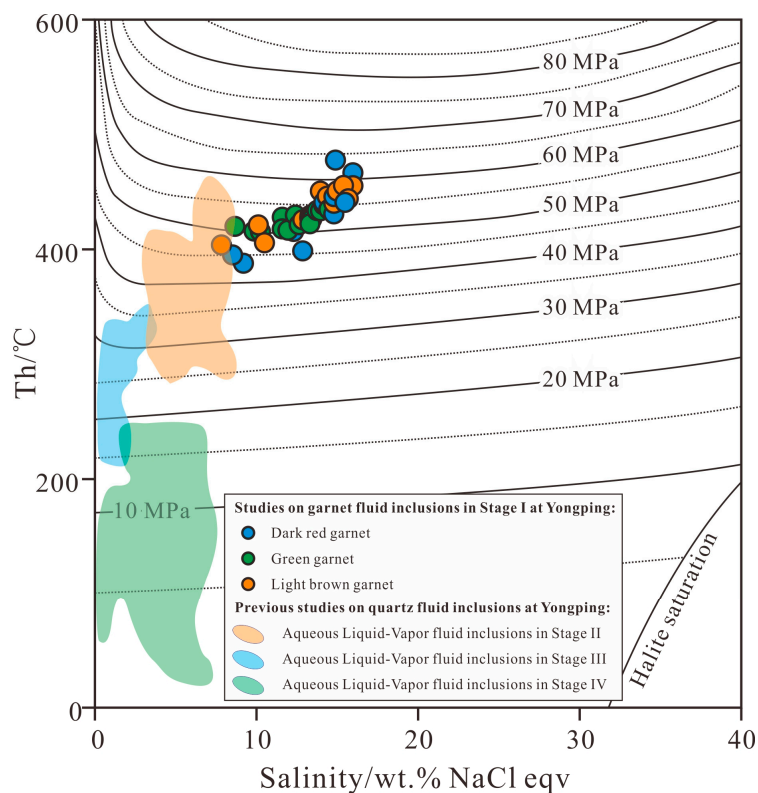
Figure 14. Homogenization temperature (Th, °C) versus salinity (wt % NaCl eqv) plots of boiling fluid inclusion assemblages from the Yongping garnets. Contours of trapping pressures (MPa) were calculated based on the correlations outlined by Driesner and Heinrich [82]. Aqueous Liquid-Vapor fluid inclusions fields were from [27]. Abbreviations: RGrt-s = zone with stronger color intensity under BSE of dark red garnet; RGrt-w = zone with weaker color intensity under BSE of dark red garnet; GGrt = green garnet; and BGrt = light brown garnet.

6.3. Metasomatic Dynamics of Yongping Garnet

Previous studies have shown that magmatic hydrothermal fluids in general have low REE contents and are LREE enriched and HREE depleted, and they usually present positive but variable Eu anomalies [11,83–86]. However, the REE patterns of garnet should not vary significantly during magmatic hydrothermal alteration because of the extremely low REE content of the hydrothermal fluid [73]. Variations in garnet geochemistry are largely controlled by external factors [11], such as water/rock (W/R) ratios and metasomatic dynamics, and only long fluid residence times or high W/R ratios can significantly change the REE patterns of garnet resulting from magmatic hydrothermal alteration [73,87]. Magmatic hydrothermal skarns form under two types of metasomatic dynamics: diffusive metasomatism or infiltration metasomatism. Diffusive metasomatism produces fluids and alteration products that present REE compositions buffered by the composition of the host rocks because of the long pore fluid residence under closed-system conditions, and these fluids have near-neutral pH, and the main complexing agents are hydroxide and carbonate [11]. In contrast, infiltration metasomatism, which is associated with an increase in W/R ratios, produces fluids and mineral assemblages buffered by mildly acidic externally derived fluids, and chloride complexes can be important in Eu^{2+} transport [11]. The Yongping garnet formed under mildly acidic pH conditions, together with the certain garnet (especially the dark red garnet) having REE patterns similar to those of common magmatic hydrothermal fluids. Therefore, we infer that this garnet formed mainly by infiltration metasomatism.

The infiltration metasomatism usually occurs when magmatic hydrothermal fluid infiltrates into the fracture zone in the carbonate strata. At Yongping, after the magmatic hydrothermal fluids

derived from Shizitou stock may have ascended, it may have preferentially entered the low-pressure fracture zones between the limestone and quartz sandstone in the Yejiawan Formation and interacted with the limestone. The interaction generated Yongping garnet in the stratiform orebodies by the infiltration metasomatism.

6.4. Implications for Yongping Mineralization

Garnet alteration favors the growth of brittle fractures in the wall rock, which can promote the migration of ore-forming hydrothermal fluids, interactions between water and rock and the formation of ore space; thus, the forming process of garnet is thought to be preparatory stage of skarn type mineralization [88,89]. Mn and Ca concentrations in garnet from the grossular–andradite solid solution series can indicate the metallogenetic potential of hydrothermal fluids [90,91]. The Yongping garnet plots in the skarn area for Au and Cu mineralization (Figure 15), which shows that the hydrothermal fluids for the Yongping garnet have the potential to produce Cu and/or Au mineralization, consistent with chalcopyrite as the main ore mineral in the Yongping deposit and the Yongping garnet plotting in the garnet area of skarn Cu deposits worldwide (Figure 8).
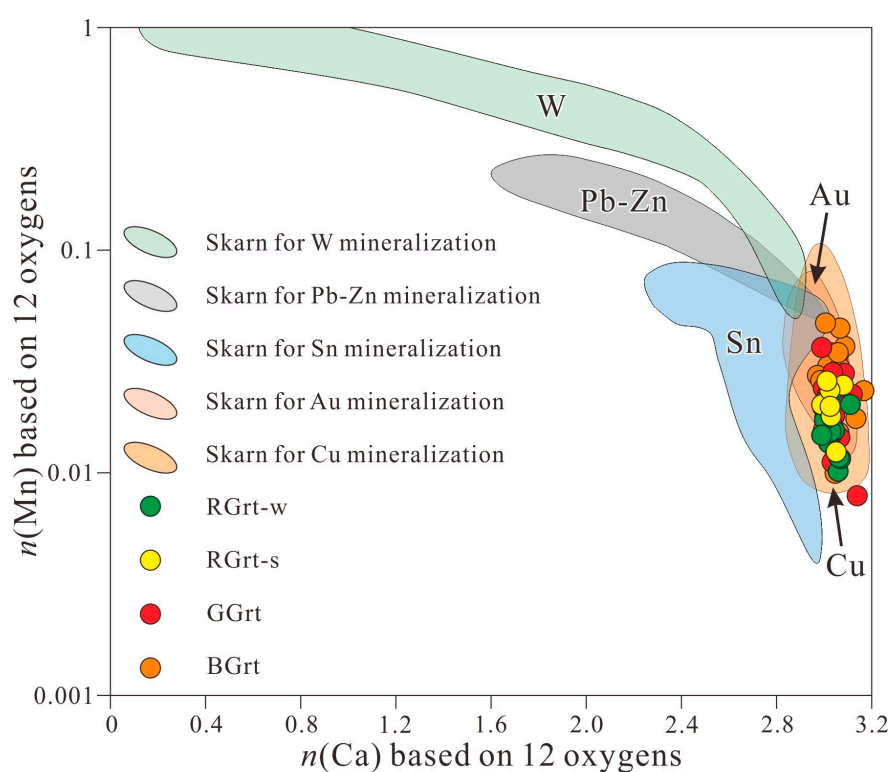
Figure 15. Discrimination diagrams of the mineralization properties for garnets in the Yongping Cu deposit (after [91]). The calculations for n(Mn) and n(Ca) are based on 12 oxygens. Abbreviations: RGrt-s = zone with stronger color intensity under BSE of dark red garnet; RGrt-w = zone with weaker color intensity under BSE of dark red garnet; GGrt = green garnet; and BGrt = light brown garnet.

The Yongping stratiform orebody is parallel with ore-hosting strata and obviously different from typical skarn-type orebody, and the stockwork mineralization at the stratiform orebodies footwall mimics the dual structure of typical sedimentary exhalative (SEDEX) deposits. These two features was interpreted to support the Hercynian submarine exhalation mineralization hypothesis [16,21,22,33–37]. However, the typical sedimentary exhalative mineralization usually response to the Zn-Pb-Ag deposit [92], rather than Cu deposit. More importantly, the footwall stockwork mineralization is dominated by pyrite-quartz veins [26,39], distinct from the mineral assemblage (such as anhydrite and

barite) in typical SEDEX footwall stockwork mineralization [92]. Moreover, the footwall alteration is dominated by silicification [26,39], inconsistent with typical SEDEX deposits, which is characterized by tourmaline, albitite, chlorite and epidote alterations [92]. Additionally, typical SEDEX deposits are characterized by syngenetic mineralization, but there is a clear abrupt contact interface between the Yongping stratiform orebody and the Yejiawang Formation quartz sandstone, indication of epigenetic mineralization [26].

Particularly, the Yongping garnet likely originated primarily via infiltration metasomatism by the magmatic-hydrothermal fluids. The fracture zones between the limestone and quartz sandstone between the Upper Carboniferous Yejiawang Formation, hosting Yongping stratiform orebodies, are corresponding to the essential open fracture system for infiltration metasomatism. The magmatic-hydrothermal fluids derived from Shizitou stock would preferentially infiltrate into the relatively low-pressure detachment zone and interacted with Yejiawang Formation carbonate to result in the Yongping garnet, which supports the magmatic-hydrothermal hypothesis for the origin of Yongping mineralization [28–32]. Therefore, we conclude that the Yongping stratiform mineralization may have been skarn-type mineralization related with Jurassic (Mesozoic) magmatic-hydrothermal fluids associated with the Shizitou stock.

7. Conclusions

(1) The Yongping garnet generally resulted from a grossular–andradite solid solution, and range from nearly pure andradite Ad_{98} to $Ad_{32}Gr_{66}$.

(2) The hydrothermal fluid that formed the Yongping garnet was under physicochemical conditions with temperatures of 387–477 °C, pressures of 44–64 MPa, mildly acidic pH levels, and unstable oxygen fugacity with enriched LREE.

(3) The Yongping garnet may have resulted from hydrothermal replacement primarily by infiltration metasomatism.

(4) The Yongping deposit represents stratiform skarn-type mineralization that is related with Jurassic magmatic-hydrothermal fluids associated with the Shizitou stock.

Author Contributions: Yu Zhang and Yongjun Shao conceived and designed the experiments; Hongbin Li performed the experiments; Yu Zhang and Qingquan Liu analyzed the data; Yu Zhang, Qingquan Liu and Yongjun Shao wrote the paper.

Conflicts of Interest: The authors declare no conflict of interest.

References

1. Meinert, L.D.; Dipple, G.M.; Nicolescu, S. World Skarn Deposits. *Econ. Geol.* **2005**, *100*, 299–336.
2. Yardley, B.W.; Rochelle, C.A.; Barnicoat, A.C.; Lloyd, G.E. Oscillatory zoning in metamorphic minerals: An indicator of infiltration metasomatism. *Mineral. Mag.* **1991**, *55*, 357–365. [CrossRef]
3. Jamtveit, B.; Wogelius, R.A.; Fraser, D.G. Zonation patterns of skarn garnets: Records of hydrothermal system evolution. *Geology* **1993**, *21*, 113–116. [CrossRef]
4. Crowe, D.E.; Riciputi, L.R.; Bezenek, S.; Ignatiev, A. Oxygen isotope and trace element zoning in hydrothermal garnets: Windows into large-scale fluid flow behavior. *Geology* **2001**, *29*, 479–482. [CrossRef]
5. Fernando, G.; Hauzenberger, C.A.; Baumgartner, L.P.; Hofmeister, W. Modeling of retrograde diffusion zoning in garnet: Evidence for slow cooling of granulites from the Highland Complex of Sri Lanka. *Mineral. Petrol.* **2003**, *78*, 53–71. [CrossRef]

6.   Smith, M.P.; Henderson, P.; Jeffries, T.E.R.; Long, J.; Williams, C.T. The rare earth elements and uranium in garnets from the Beinn and Dubhaich Aureole, Skye, Scotland, UK: Constraints on processes in a dynamic hydrothermal system. *J. Petrol.* **2004**, *45*, 457–484. [CrossRef]

7.   Kim, H.S. Deformation-induced garnet zoning. *Gondwana Res.* **2006**, *10*, 379–388. [CrossRef]

8.   Martin, L.A.J.; Ballèvre, M.; Boulvais, P.; Halfpenny, A.; Vanderhaeghe, O.; Duchêne, S.; Deloule, E. Garnet re-equilibration by coupled dissolution-reprecipitation: Evidence from textural, major element and oxygen isotope zoning of 'cloudy' garnet. *J. Metamorph. Geol.* **2011**, *29*, 21–231. [CrossRef]

9.   Scherer, E.E.; Cameron, K.L.; Blichert-Toft, J. Lu-Hf garnet geochronology: Closure temperature relative to the Sm-Nd system and the effects of tracemineral inclusions. *Geochim. Cosmochim. Acta* **2000**, *64*, 3413–3432. [CrossRef]

10. Pertermann, M.; Hirschmann, M.M.; Hametner, K.; Günther, D.; Schmidt, M.W. Experimental determination of trace element partitioning between garnet and silica-rich liquid during anhydrous partial melting of MORB-like eclogite. *Geochem. Geophys. Geosyst.* **2004**, *5*, 297–319. [CrossRef]

11. Gaspar, M.; Knaack, C.; Meinert, L.D.; Moretti, R. REE in skarn systems: A LA–ICP-MS study of garnets from the Crown Jewel gold deposit. *Geochim. Cosmochim. Acta* **2008**, *72*, 185–205. [CrossRef]

12. Schmidt, A.; Mezger, K.; O'Brien, P.J. The time of eclogite formation in the ultrahigh pressure rocks of the Sulu terrane: Constraints from Lu–Hf garnet geochronology. *Lithos* **2011**, *125*, 743–756. [CrossRef]

13. Cheng, H.; Zhang, C.; Vervoort, J.D.; Lu, H.H.; Wang, C.; Cao, D.D. Zircon U-Pb and garnet Lu-Hf geochronology of eclogites from the Lhasa Block, Tibet. *Lithos* **2012**, *155*, 341–359. [CrossRef]

14. Somarin, A.K. Garnet composition as an indicator of Cu mineralization: Evidence from skarn deposits of NW Iran. *J. Geochem. Explor.* **2004**, *81*, 47–57. [CrossRef]

15. Zhai, D.G.; Liu, J.J.; Zhang, H.Y.; Wang, J.P.; Su, L.; Yang, X.A.; Wu, S.H. Origin of oscillatory zoned garnets from the Xieertala Fe–Zn skarn deposit, northern China: In situ LA–ICP-MS evidence. *Lithos* **2014**, *190*, 279–291. [CrossRef]

16. Gu, L.X.; Zaw, K.; Hu, W.X.; Zhang, K.J.; Ni, P.; He, J.X.; Xu, Y.T.; Lu, J.J.; Lin, C.M. Distinctive features of Late Paleozoic massive sulfide deposits in South China. *Ore Geol. Rev.* **2007**, *31*, 107–138. [CrossRef]

17. Xu, Y.T. The characteristics of genetical geochemistry of cherts in Yongping copper deposit, Jiangxi Province. *Geotecton. Metallog.* **1996**, *20*, 20–28. (In Chinese)

18. Li, X.H.; McCulloch, M.T. Secular variation in the Nd isotopic composition of Neoproterozoic sediments from the southern margin of the Yangtze block: Evidence for a Proterozoic continental collision in southeast China. *Precambrian Res.* **1996**, *76*, 67–76. [CrossRef]

19. Liu, X.; Huang, Z. The discussion on the development of structures at Yongping Cu deposit in Jiangxi Province. *Miner. Resour. Geol.* **1991**, *6*, 416–422. (In Chinese)

20. Lu, C.H. Ore Source and Mineralization of Molybdenum in Copper Deposit in Yongping, Jiangxi. *J. East China Coll. Geol.* **1986**, *9*, 116–127. (In Chinese)

21. Chen, Y.F. The Metallogenic Material Source and Genesis of the Yongping Copper Deposit. *Nonferrous Met.* **2004**, *56*, 19–21. (In Chinese)

22. Du, L.T. Sources of ore–forming material and genesis analysis of Yongping Copper Deposit, Jiangxi. *Hubei Geol. Miner. Resour.* **2005**, *19*, 4–11. (In Chinese)

23. Luo, P. Metallogenetic Regularities and Prediction of Copper-Lead-Zinc-Silver Mineralization in the Area of Chenfang-Yongping, Yanshan County, Jiangxi Province. Master's Thesis, China University of Geosciences, Wuhan, China, 2005. (In Chinese)

24. Li, H.X. The Appraisal of Favorableness to Ore–Forming of Copper and Polymetallic Ore in Yongping of Jiangxi Province. Master's Thesis, Hefei University of Technology, Hefei, China, 2009. (In Chinese)

25. Cao, D.H. *Internal Research Report: Metallogenetic Regularities of Shizitou Mo Deposit, Yongping, Jiangxi Province, China*; Chinese Academy of Geological Sciences: Beijing, China, 2012. (In Chinese)

26. Shao, Y.J.; Zhang, Y.; Quan, W.; Luo, M.Y. *Internal Research Report: Deep Ore Prospecting for Yongping Cu Deposit, Jiangxi Province, China*; Central South University: Changsha, China, 2015. (In Chinese)

27. Zhu, X.T.; Ni, P.; Wang, G.G.; Cai, Y.T.; Chen, H.; Pan, J.Y. Fluid inclusion, H-O isotope and Pb-Pb age constraints on the genesis of the Yongping copper deposit, South China. *J. Geochem. Explor.* **2016**. [CrossRef]

28. He, J. Discussion on skarn genesis of Yongping copper deposit. *J. Sichuan Inst. Build. Mater.* **1989**, *4*, 31–40. (In Chinese)

29. He, J. Metallogenic geochemistry and genesis study on Yongping copper ore deposit of Jiangxi Province. *Miner. Resour. Geol.* **1993**, *7*, 1–7. (In Chinese)

30. Ding, X.; Jiang, S.Y.; Ni, P.; Gu, L.X.; Jiang, Y.H. Zircon SIMS U-Pb geochronology of host granitoids in Wushan and Yongping copper deposits, Jiangxi Province, China. *Geol. J. China Univ.* **2005**, *11*, 383–389. (In Chinese)

31. Zhu, B.; Jiang, S.Y.; Ding, X.; Jiang, Y.H.; Ni, P.; Gu, L.X. Hydrothermal Alteration and Petrogenesis of Granites in the Yongping Copper Deposit, Jiangxi Province: Constraints from Mineral Chemistry, Element Geochemistry, and Sr–Nd–Hf Isotopes. *Acta Petrol. Sin.* **2008**, *24*, 1900–1916. (In Chinese)

32. Mao, J.W.; Chen, M.H.; Yuan, S.D.; Guo, C.L. Geological Characteristics of the Qin-Hang (or Shihang) Metallogenic Belt in South China and Spatial-Temporal Distribution Regularity of Mineral Deposits. *Acta Petrol. Sin.* **2011**, *85*, 636–658. (In Chinese)

33. Ren, J.G. Tectonic mineralization and genesis of Yongping copper deposit, Jiangxi Province. *Copp. Eng.* **1994**, *3*, 35–40. (In Chinese)

34. Ren, J.G. The characteristics and genesis of molybdenum mineralization in Yongping. *Copp. Eng.* **1996**, *3*, 40–44. (In Chinese)

35. Zhang, Z.S.; Zhu, M.Q. Geochemical Evidence of Sedimentary Exhalation Mineralization of Yongping Copper Deposits. *Miner. Depos.* **2002**, *21*, 545–547. (In Chinese)

36. Liao, Z.T.; Liu, J.S. Evidence of submarine volcanic hydrothermal sediment mineralization in Yongping copper deposit. *Copp. Eng.* **2003**, *1*, 31–35. (In Chinese)

37. Ni, P.; Tian, J.H.; Zhu, X.T.; Ling, H.F.; Jiang, S.Y.; Gu, L.X. Fluid inclusion studies on footwall stringer system mineralization of Yongping massive copper deposit, Jiangxi Province, China. *Acta Petrol. Sin.* **2005**, *21*, 1339–1346. (In Chinese)

38. Tian, M.J.; Li, Y.G.; Wan, H.Z.; Zhang, Y.; Gao, T.T. Characteristics of skarn minerals in Yongping copper deposit, Jiangxi Province, and geological significances. *Acta Petrol. Sin.* **2014**, *30*, 3741–3758. (In Chinese)

39. Luo, M.Y. Characteristics of the Ore–Forming Hydrothermal Fluid in Yongping Cu-Mo Ore Field, Jiangxi Province, Southern China. Master's Thesis, Central South University, Changsha, China, 2016. (In Chinese)

40. Einaudi, M.T.; Burt, D.M. Introduction-terminology, classification, and composition of skarn deposits. *Econ. Geol.* **1982**, *77*, 745–754. [CrossRef]

41. Doyle, M.G.; Allen, R.L. Subsea-floor replacement in volcanic-hosted massive sulfide deposits. *Ore Geol. Rev.* **2003**, *23*, 183–222. [CrossRef]

42. Zhang, X.S. Characteristics of Chemical Composition and Mineral Inclusions of Ore Minerals in Yongping Copper Deposit. *Jiangxi Geol.* **1997**, *11*, 40–48. (In Chinese)

43. Tian, J.H.; Ni, P.; Fan, J.G. Ore–forming fluid characteristics research of Yongping copper deposit. *Contrib. Mineral. Petrol.* **2001**, *16*, 24–27. (In Chinese)

44. Shui, T.; Xu, B.T.; Liang, R.H.; Qiu, Y.S. Paleo-continent building belt in Shaoxing-Jiangshan. *Chin. Sci. Bull.* **1986**, *6*, 444–448. (In Chinese)

45. Wang, X.L.; Zhou, J.C.; Griffin, W.L.; Wang, R.C.; Qiu, H.S.; O'Reilly, S.Y.; Xu, X.S.; Liu, X.M.; Zhang, G.L. Detrital zircon geochronology of Precambrian basement sequences in the Jiangnan orogen: Dating the assembly of the Yangtze and Cathaysia Blocks. *Precambrian Res.* **2007**, *159*, 117–131. [CrossRef]

46. Mao, J.W.; Cheng, Y.B.; Chen, M.H.; Pirajno, F. Major types and time-space distribution of Mesozoic ore deposits in South China and their geodynamic settings. *Miner. Depos.* **2013**, *48*, 267–294.

47. Zhao, C.; Ni, P.; Wang, G.G.; Ding, J.Y.; Chen, H.; Zhao, K.D.; Cai, Y.T.; Xu, Y.F. Geology, fluid inclusion, and isotope constraints on ore genesis of the Neoproterozoic Jinshan orogenic gold deposit, South China. *Geofluids* **2013**, *13*, 506–527. [CrossRef]

48. Zhou, X.M.; Sun, T.; Shen, W.Z.; Shu, L.S.; Niu, Y.L. Petrogenesis of Mesozoic granitoids and volcanic rocks in South China: A response to tectonic evolution. *Episodes* **2006**, *29*, 26–33.

49. Wang, G.G.; Ni, P.; Yu, W.; Chen, H.; Jiang, L.L.; Li, P.F. Petrogenesis of Early Cretaceous post-collisional granitoids at Shapinggou, Dabie Orogen: Implications for crustal architecture and porphyry Mo mineralization. *Lithos* **2014**, *184–187*, 393–415. [CrossRef]

50. Zhang, H.; Ling, M.M.; Liu, Y.L.; Tu, X.L.; Wang, F.Y.; Li, C.Y.; Liang, H.Y.; Yang, X.Y.; Arndt, N.T.; Sun, W.D. High oxygen fugacity and slab melting linked to Cu mineralization: Evidence from Dexing porphyry copper deposits, Southeastern China. *J. Geol.* **2013**, *121*, 289–305. [CrossRef]

51. Wang, T.G.; Ni, P.; Wang, G.G.; Zhang, T. Identification and significance of methanerich fluid inclusions in changba Pb-Zn deposit, Gansu province. *Acta Petrol. Sin.* **2008**, *24*, 2105–2112. (In Chinese)

52. Li, L.M.; Sun, M.; Wang, Y.; Xing, G.; Zhao, G.; He, Y.; He, K.; Zhang, A. U-Pb and Hf isotopic study of detrital zircons from the meta-sedimentary rocks in central Jiangxi Province, South China: Implications for the Neoproterozoic tectonic evolution of South China Block. *J. Asian Earth Sci.* **2011**, *41*, 44–55. [CrossRef]

53. Li, L.M.; Sun, M.; Wang, Y.; Xing, G.; Zhao, G.; Lin, S.; Xia, X.; Chan, L.; Zhang, F.; Wong, J. U-Pb and Hf isotopic study of zircons from migmatised amphibolites in the Cathaysia Block: Implications for the early Paleozoic peak tectonothermal event in Southeastern China. *Gondwana Res.* **2011**, *19*, 191–201. [CrossRef]

54. Qin, X.F. A Preliminary Framework for the Sequence of Volcanic-Intrusive Magma of Relation to Mineralization in the North Wuyi Yanshanian Area. Master's Thesis, China University of Geosciences, Beijing, China, 2014. (In Chinese)

55. Yu, D.; Ye, F.; Wang, Y. Active succession establishment for volcanic-intrusive complex in Middle-Late lower Cretaceous in Guangfeng, Jiangxi and its geological implication. *Geotecton. Metallog.* **2001**, *25*, 271–276. (In Chinese)

56. Wang, G.G.; Ni, P.; Zhao, K.D.; Wang, X.L.; Liu, J.Q.; Jiang, S.Y.; Chen, H. Petrogenesis of the Middle Jurassic Yinshan volcanic-intrusive complex, SE China: Implications for tectonic evolution and Cu-Au mineralization. *Lithos* **2012**, *150*, 135–154. [CrossRef]

57. Zhang, Z.H. *Large-Scale Metauogenic Prognosis for Concealed Deposits in Northeastern Jiangxi*; Geological Publishing House: Beijing, China, 1996. (In Chinese)

58. Jiang, Y.H.; Zhao, P.; Zhou, Q.; Liao, S.Y.; Jin, G.D. Petrogenesis and tectonic implications of Early Cretaceous S- and A-type granites in the northwest of the Gan-Hang rift, SE China. *Lithos* **2011**, *121*, 55–73. [CrossRef]

59. Quan, W. Petrogenesis of Shizitou Granites in Yongping Cu-Mo deposit, Jiangxi Province. Master's Thesis, Central South University, Changsha, China, 2015. (In Chinese)

60. Luo, P. Research on Metallogenic Regularities and Prospecting Orientation of Copper Polymetal Mineral Resources in the Northern Wuyi Region of Jiangxi Province. Ph.D. Thesis, China university of Geosciences, Beijing, China, 2010. (In Chinese)

61. Liu, Y.S.; Gao, S.; Hu, Z.C.; Gao, C.G.; Zong, K.Q.; Wang, D.B. Continental and oceanic crust recycling-induced melt-peridotite interactions in the Trans-North China Orogen: U-Pb dating, Hf isotopes and trace elements in zircons of mantle xenoliths. *J. Petrol.* **2010**, *51*, 537–571. [CrossRef]

62. Brown, P.E. FLINCOR: A microcomputer program for the reduction and investigation of fluid inclusion data. *Am. Mineral.* **1989**, *74*, 1390–1393.

63. Meinert, L.D. Skarns and skarn deposits. *Geosci. Can.* **1992**, *19*, 145–162.

64. Zhang, Y.; Shao, Y.J.; Wu, C.D.; Chen, H.Y. LA-ICP-MS trace element geochemistry of garnets: Constraints on hydrothermal fluid evolution and genesis of the Xinqiao Cu–S–Fe–Au deposit, eastern China. *Ore Geol. Rev.* **2017**, *86*, 426–439. [CrossRef]

65. Sun, S.; McDonough, W.F. Chemical and isotopic systematics of oceanic basalts: Implications for mantle composition and processes. In *Magmatism in the Ocean Basins*; The Geological Society of London: London, UK, 1989; Volume 42, pp. 313–345.

66. Gemmell, J.B.; Zantop, H.; Meinert, L.D. Genesis of the Aguilar zinc-lead-silver deposit, Argentina; contact metasomatic vs. sedimentary exhalative. *Econ. Geol.* **1992**, *87*, 2085–2112. [CrossRef]

67. Burton, K.W.; Bourdon, B.; Birck, J.L.; Allègre, C.J.; Hein, J.R. Osmium isotope variations in the oceans recorded by Fe Mn crusts. *Earth Planet. Sci. Lett.* **1999**, *171*, 185–197. [CrossRef]

68. Ling, Q.C.; Cheng, H.L. Discussion on forming process and geological characteristics of magmatic skarn in Tongling area, Anhui Province. *J. Changchun Univ. Sci. Technol.* **1998**, *28*, 366–371. (In Chinese)

69. Xiao, C.D.; Liu, X.W. REE geochemistry and origin of skarn garnets from eastern Inner Mongolia. *Geol. China* **2002**, *29*, 311–316. (In Chinese)

70. Zheng, Z.; Du, Y.S.; Cao, Y.; Cao, Z.W.; Yang, S.; Dong, Q. The composition characteristics and origin of garnets in the Dongguashan skarn copper deposit, Anhui Province, China. *Acta Petrol. Mineral.* **2012**, *31*, 235–242. (In Chinese)

71. Bau, M.; Dulski, P. Anthropogenic origin of positive gadolinium anomalies in river waters. *Earth Planet. Sci. Lett.* **1996**, *143*, 245–255. [CrossRef]

72. Anders, M.; Grevesse, N. Abundances of the elements: Meteoritic and solar. *Geochim. Cosmochim. Acta* **1989**, *53*, 197–214. [CrossRef]

73. Bau, M. Rare-earth element mobility during hydrothermal and metamorphic fluid-rock interaction and the significance of the oxidation state of europium. *Chem. Geol.* **1991**, *93*, 219–230. [CrossRef]

74. Mayanovic, R.A.; Jayanetti, S.; Anderson, A.J.; Bassett, W.A.; Chou, I.M. The structure of Yb^{3+} aquo ion and chloro complexes in aqueous solutions at up to 500 °C and 270 MPa. *J. Phys. Chem. A* **2002**, *106*, 6591–6599. [CrossRef]

75. Allen, D.E.; Seyfried, W.E. REE controls in ultramafic hosted MOR hydrothermal systems: An experimental study at elevated temperature and pressure. *Geochim. Cosmochim. Acta* **2005**, *69*, 675–683. [CrossRef]

76. Gaspar, M. The Crown Jewel Gold Skarn Deposit. Ph.D. Thesis, Washington State University, Pullman, WA, USA, 2005.

77. Sverjensky, D.M. Europium redox equilibria in aqueous solution. *Earth Planet. Sci. Lett.* **1984**, *67*, 70–78. [CrossRef]

78. Shannon, R.D. Revised effective ionic radii and systematic studies of interatomic distances in halides and chalcogenides. *Acta Crystallogr.* **1976**, *32*, 751–767. [CrossRef]

79. Dziggel, A.; Wulff, K.; Kolb, J.; Meyer, F.M.; Lahaye, Y. Oscillatory zoning in metamorphic minerals: An indicator of infiltration metasomatism. *Chem. Geol.* **2009**, *262*, 262–276. [CrossRef]

80. Meinert, L.D. Application of skarn deposit zonation models to mineral exploration. *Explor. Min. Geol.* **1997**, *6*, 185–208.

81. Roedder, E. The fluids in salt. *Am. Mineral.* **1984**, *69*, 413–439.

82. Driesner, T.; Heinrich, C.A. The system H_2O–NaCl. Part I: Correlation formulae for phase relations in temperature–pressure–composition space from 0 to 1000 °C, 0 to 5000 bar, and 0 to 1 X_{NaCl}. *Geochim. Cosmochim. Acta* **2007**, *71*, 4880–4901. [CrossRef]

83. Flynn, R.T.; Burnham, W. An experimental determination of rare earth partition coefficients between a chloride containing vapour phase and silicate melts. *Geochim. Cosmochim. Acta* **1978**, *42*, 685–701. [CrossRef]

84. Ayers, J.C.; Eggler, D.H. Partitioning of elements between silicate melt and H_2O-NaCl fluids at 1.5 and 2.0 GPa pressure: Implications for mantle metasomatism. *Geochim. Cosmochim. Acta* **1995**, *59*, 4237–4246. [CrossRef]

85. Kravchuk, I.F.; Ivanova, G.F.; Varezhkina, N.S.; Malinin, S.D. REE fractionation in acid fluid-magma systems. *Geochem. Int.* **1995**, *32*, 60–68.

86. Reed, M.J.; Candela, P.A.; Piccoli, P.M. The distribution of rare earth elements between monzogranitic melt and the aqueous volatile phase in experimental investigations at 800 °C and 200 MPa. *Contrib. Mineral. Petrol.* **2000**, *140*, 251–262. [CrossRef]

87. Lottermoser, B.G. Rare earth elements and hydrothermal ore formation processes. *Ore Geol. Rev.* **1992**, *7*, 25–41. [CrossRef]

88. Karimzadeh, S.A. Garnetization as aground preparation process for copper mineralization: Evidence from the Mazraeh skarn deposit, Iran. *Int. J. Earth Sci.* **2010**, *99*, 343–356. [CrossRef]

89. Ying, L.J.; Tang, J.X.; Wang, D.H.; Wang, W.P. Features of garnet in the Jiama super-large Cu polymetallic deposit and its genetic significance. *Acta Geol. Sin.* **2012**, *86*, 1735–1747. (In Chinese)

90. Ray, G.E.; Webster, B.C.; Ettlinger, A.D. The distribution of skarns in British Columbia and the chemistry and ages of their related plutonic rocks. *Econo. Geol.* **1995**, *90*, 920–937. [CrossRef]

91. Qin, Z.P.; Tang, X.Q.; Zhou, Y.; Song, L. Geochemical characteristics and metallogenic significances of the three garnets in Jiama Cu-polymetallic deposit, Tibet. *Nonferrous Met.* **2013**, *65*, 22–26. (In Chinese)

92. Sangester, D.F. Mississippi Valley-type and SEDEX lead-zinc deposits: A comparative examination. *Trans. Inst. Min. Metall. B Appl. Earth Sci.* **1990**, *99*, 21–42.